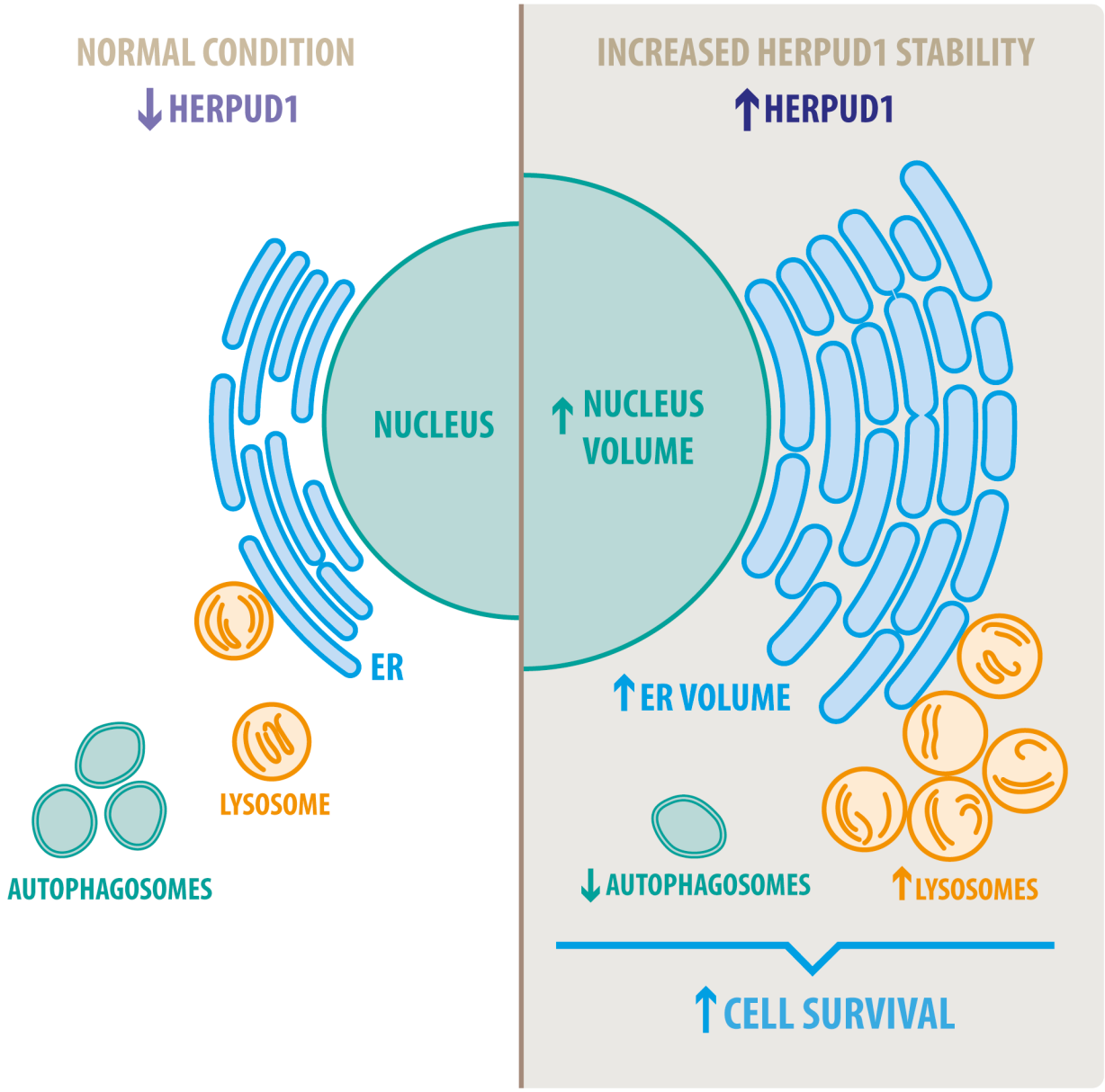
NORMAL CONDITION
HERPUD1
NUCLEUS
ER
LYSOSOME
AUTOPHAGOSOMES
INCREASED HERPUD1 STABILITY
HERPUD1
NUCLEUS VOLUME
ER VOLUME
AUTOPHAGOSOMES
LYSOSOMES
CELL SURVIVAL

Negative modulation of macroautophagy by HERPUD1 is counteracted by an increased ER-lysosomal network with impact in drug-induced stress cell survival

Vargas G.[1ǂ], Cortés O.[1ǂ], Arias-Muñoz E.[1,2], Hernández S.[1], Cerda-Troncoso C.[1], Hernández L.[1], González A. E.[5]&, Tatham M. H.[3], Bustamante H.[4], Retamal C.[1], Cancino J.[1], Varas-Godoy M.[1], Hay R. T.[3], Rojas-Fernandez A.[3,6], Cavieres V. A.[1,2*] and Burgos P. V.[1,2*]

[1] Centro de Biología Celular y Biomedicina (CEBICEM), Facultad de Medicina y Ciencia, Universidad San Sebastián, Lota 2465, Santiago 7510157, Chile.

[2] Centro de Envejecimiento y Regeneración (CARE-UC), Facultad de Ciencias Biológicas, Pontificia Universidad Católica, Santiago 8330023, Chile

[3] Center for Gene Regulation and Expression, College of Life Sciences, University of Dundee, DD1 4HN, Dundee 4HN UK

[4] Instituto de Microbiología Clínica, Facultad de Medicina, Universidad Austral de Chile, Valdivia 5110566, Chile.

[5] Instituto de Fisiología, Facultad de Medicina, Universidad Austral de Chile, Valdivia 5110566, Chile.

[6] Instituto de Medicina & Centro Interdisciplinario de Estudios del Sistema Nervioso (CISNe), Universidad Austral de Chile, Valdivia 5110566, Chile.

[*] Correspondence: vcavieresr@docente.uss.cl (V.A.C.); patricia.burgos@uss.cl (P.V.B.); Tel.: +56-9-65887097 (V.A.C.); +56-2-22606309 (P.V.B.)

[ǂ] These authors contributed equally to this work

[&] Current address: Institute of Biochemistry II, School of Medicine, Goethe University Frankfurt, Theoder-Stern-Kai 7, 60590 Frankfurt am Main, Germany.

ABSTRACT

Macroautophagy and the ubiquitin proteasome system work as an interconnected network in the maintenance of cellular homeostasis. Indeed, efficient activation of macroautophagy upon nutritional deprivation is sustained by degradation of preexisting proteins by the proteasome. However, the specific substrates that are degraded by the proteasome in order to activate macroautophagy are currently unknown. By quantitative proteomic analysis we identified several proteins downregulated in response to starvation but independently of ATG5 expression. Among them, the most significant was HERPUD1, an ER protein of short-half life and a well-known substrate of the proteasome. We found that increased HERPUD1 stability by deletion of its ubiquitin-like domain (UBL) plays a negative role on basal and induced macroautophagy. Moreover, we found it triggers ER expansion by reordering the ER in crystalloid structures, but in the absence of unfolded protein response activation. Surprisingly, we found ER expansion led to an increase in the number and function of lysosomes establishing a tight network with the presence of membrane-contact sites.

Importantly, a phosphomimetic S59D mutation within the UBL mimics UBL deletion on its stability and the ER-lysosomal network expansion revealing an increase of cell survival under stress conditions. Altogether, we propose stabilized HERPUD1 downregulates macroautophagy favoring instead a closed interplay between the ER and lysosomes with consequences in drug-cell stress survival.

INTRODUCTION

Macroautophagy (from here referred to as autophagy) is a catabolic pathway that mediates the engulfment of aberrant or damaged cytoplasmic constituents into double-membrane autophagosomes that subsequently fuse with lysosomes to form a hybrid organelle called the autolysosome that mediates the degradation of the cargo by acid hydrolases (Mizushima et al. 2008; Khaminets, Behl, and Dikic 2016). Autophagy is also implicated in the degradation of cellular constituents under basal conditions, playing an essential role in the maintenance of cellular homeostasis upon a variety of environmental conditions such as nutrient restriction or other stressors (Murrow and Debnath 2013). Autophagy is highly inducible by environmental changes being a highly dynamic process that resolves a variety of cellular demands (Murrow and Debnath 2013). In fact, increased autophagy is protective in different cells and organisms, playing a crucial role in cell maintenance and survival under different insults (Moreau, Luo, and Rubinsztein 2010). On the other hand, defects in autophagy enhance cell vulnerability under harmful conditions such as those present in the tumor microenvironment (Camuzard et al. 2020).

Although initially autophagy was thought to work independently of the ubiquitin proteasome system (UPS), increasing evidence shows many layers of both negative and positive regulation (Bustamante et al. 2018), revealing an interconnected network with important roles in cellular homeostasis and maintenance (Korolchuk, Menzies, and Rubinsztein 2010). Inhibitors of the proteasome 20S catalytic core with the use of β-subunits blockers triggers an enhancement in the biogenesis of autophagosomes (Zhu, Dunner, and McConkey 2010). In contrast, impairment of the proteasome 19S regulatory particle with an inhibitor of PSMD14, a proteasomal deubiquitinating enzyme, blocks the biogenesis of autophagosomes (Demishtein et al. 2017; Bustamante et al. 2020). To date a limited number of substrates of the UPS system are known to play a regulatory role in autophagy (Jia and Bonifacino 2019; Thayer et al. 2020) and many aspects about the functional role of this interconnected network between autophagy and UPS remain elusive.

To identify UPS substrates that could act as negative regulators of autophagy, we conducted a quantitative SILAC proteomic analysis in cells stably depleted of ATG5 by shRNA-mediated knockdown. ATG5 protein is part of a complex with ATG12 and ATG16L that controls an essential step in the autophagosome formation (Walczak and Martens 2013). We focused on proteins downregulated in response to nutrient deprivation, but not because of autophagy activation. The protein with the most significant downregulation, in wild type and ATG5 depleted cells was the Homocysteine-responsive endoplasmic reticulum-resident ubiquitin-like domain (UBL) member 1 protein named as HERPUD1. This protein is a transmembrane ER-resident protein with low levels of expression due to its short half-life by rapid proteasomal degradation (K. Kokame et al. 2000; Sai et al. 2003).

Here, we found that increased HERPUD1 stability through the deletion of its UBL domain causes a decrease in basal and induced autophagy. Additionally, it promotes an ER expansion which is organized in stacked tubules forming crystalloid ER-like structures but independent of ER stress. Furthermore, we uncovered that higher HERPUD1 stability has a positive impact in lysosomal function, establishing an ER-lysosomal network with the presence of membrane contact-sites (MCS). Further, combining bioinformatics and site-directed mutagenesis we found the phosphomimetic S59D mutant within the UBL domain of HERPUD1 mimics the effect of the UBL deletion increasing its levels and inducing the expansion of the ER-lysosomal network, a phenotype that promotes stress cell survival. These findings thus identify HERPUD1 as a hotspot platform to promote stress cell survival by inducing an expansion of the ER-lysosomal network when autophagy slows down.

MATERIALS AND METHODS

Reagents

Bafilomycin A1 (BafA1, cat#B1793), tunicamycin (Tun, cat#T7765), thapsigargin (Tg, cat#T9033), cisplatin (CDDP, cat#479306), Sulforhodamine B (SRB, cat#230162), Earle's balanced salt solution (EBSS, Cat#E2888), puromycin dihydro-chloride (cat#P8833), and protease inhibitors cocktail (cat#P8340) were purchased from Sigma-Aldrich (St. Louis, MO, USA). MG132 (cat#474790) was purchased from Merck Millipore (Burlington, MA, USA). LysoTracker™ Red DND-99 (cat#L7528), 4′,6-diamidino-2-phenylindole (DAPI) (cat#D-1306) and TRIzol™ (cat#15596018) were purchased from ThermoFisher Scientific (Waltham, MA, USA), Magic Red® (cat#6133) was purchased from Immunochemistry Technologies, LLC (Bloomington, IN, USA). The QuikChange II XL direct-mutagenesis kit was obtained from Stratagene (cat#200522, La Jolla, CA, USA) and the Vybrant Apoptosis Pacific Blue-annexin V kit and 7AAD from Invitrogen (cat#A35122).

Antibodies

The following monoclonal antibodies were used: mouse anti-β-ACTIN clone BA3R (cat# MA5-15739, Thermo Fisher Scientific), mouse anti-XBP-1S clone E7M5C (cat#47134S, Cell Signaling Technology, Danvers, MA, USA), mouse anti-FLAG clone M2 (cat#F1804, Sigma Aldrich), mouse anti-GRP78/BiP clone 40/BiP (cat# 610978, BD Biosciences, San Jose, CA, USA), mouse anti-LAMP1 clone H4A3 (cat# 610978, Developmental Studies Hybridoma Bank, Iowa City, IA, USA), rabbit monoclonal anti-CALNEXIN clone C5C9 (cat#2679S, Cell Signaling Technologies), rabbit monoclonal anti-ATF4 clone D4B8 (cat#11815S, Cell Signaling Technologies), rabbit monoclonal anti-HERPUD1 clone EPR9649 (cat#ab150424, Abcam), rat monoclonal anti-GRP94 clone SPM249 (cat#ab233979, Abcam, Cambridge, UK). We used the following polyclonal antibodies: rabbit anti-LC3 (cat#2775S, Cell Signaling Technology), rabbit anti-PERK (cat#P0074, Sigma-Aldrich), goat anti-CATHEPSIN-D (cat#AF1014, R&D Systems, Minneapolis, MN, USA), rabbit anti-HERPUD1 (cat#BML-PW9705, ENZO Life Sciences, Farmingdale, NY, USA). Horseradish peroxidase-conjugated secondary antibodies were purchased from Jackson ImmunoResearch Laboratories (West Grove, PA, USA), Alexa fluorophore-conjugated secondary antibodies were purchased from Thermo Fisher Scientific.

Mass Spectrometry based proteomics and statistical analysis

137 Human H4 neuroglioma cells stably expressing shLuc and shATG5 were grown in
138 Dulbecco's modified Eagle's medium lacking all amino acids except L-lysine and L-arginine,
139 which were replaced with either unlabelled amino-acids (Lys0 and Arg0) or stable isotopic
140 forms 13C6 15N2-lysine (Lys8) and 13C6 15N4-arginine (Arg10) (Cambridge Isotope
141 Laboratories). The medium was supplemented with 10% dialyzed FBS using previous
142 published methods (Golebiowski et al. 2009; Yin et al. 2012). Two separate cultures of each
143 shLuc and shATG5 cells were grown in light amino acids (Lys0 + Arg0) or heavy amino
144 acids (Lys8 + Arg10) over 9 replication cycles to achieve over 96% incorporation and similar
145 cell counts per culture. Both cell cultures were divided in two, and cells were grown under
146 control conditions in DMEM + 10% FBS or starvation in EBSS media for 4 h so that each cell
147 type grown with each label were treated with both conditions (8 cultures in total). Cells were
148 washed and lysed in 1.2 x LDS sample buffer with reducing agent, obtaining crude cell
149 extracts at approximately 1mg/ml. To allow all experimental conditions to be compared with
150 one another a light reference mix was obtained by combining all four light amino acid
151 conditions in a 1:1:1:1 ratio by volume. This was then mixed 1:1 ratio (v:v) with each heavy
152 amino acid extract. The same comparisons were made in reverse by combining all heavy
153 amino acid samples into a reference mix and combining this 1:1 (v:v) with each of the four
154 individual light amino acid conditions. See Figure 1A for experimental design. All 8 mixes
155 were fractionated by SDS-PAGE and stained gels were cut into 3 slices per lane before
156 tryptic peptides were extracted. The resultant 24 samples of dried down peptides were
157 resuspended in 35 µl 0.1% TFA 0.5% acetic acid. Peptide samples were analyzed by LC-
158 MS/MS twice; the first using 9 µl peptide sample run over a 90 min peptide fractionation
159 gradient, and the second using 18 µl peptide sample run over a 240 min fractionation
160 gradient. Peptides were analyzed using a Q exactive mass spectrometer (Thermo Scientific)
161 coupled to an EASY-nLC 1000 liquid chromatography system (Thermo Scientific), using an
162 EASY-Spray ion source (Thermo Scientific), running a 75 µm x 500 mm EASY-Spray column
163 at 45ºC. A top 10 data-dependent method was applied. Full scan spectra (m/z 300-1800)
164 were acquired with resolution R= 70,000 at m/z 200 (after accumulation to a target value of
165 1,000,000 with maximum injection time of 20ms). The most intense ions were fragmented by
166 HCD and measured with a resolution of R= 17,500 at m/z 200 (target value of 500,000
167 maximum injection time of 60 ms) and intensity threshold of $2.1x10^4$. Peptide match was set
168 to “preferred”, a 40 second dynamic exclusion list was applied, and ions were ignored if they
169 had an assigned charge state of 1, 8 or >8. All 48 data files were analyzed simultaneously in
170 MaxQuant (v1.5.2.8) using default parameters excepting the selection of SILAC labels,
171 activation of ‘requantify’ and ‘match between runs’, using a uniport ‘HUMAN’ proteome
172 database (downloaded 24/02/2015- 73920 entries) as search space. Raw files derived from
173 the same mix were grouped under the ‘Experiment’ heading as Mix01-Mix08. Raw files were
174 given MaxQuant experimental design ‘fraction’ numbers such that spectra derived from the
175 same HPLC gradient and from the equivalent gel slices across different lanes would be
176 matched, as well as one sliced either side. 4395 protein groups were listed as informed in
177 the Supp. File 1, proteinGroups.txt sheet. This list was edited to leave 3911 protein groups
178 by removing decoy proteins, protein listed as potential contaminants, proteins identified only
179 by modified peptides, and proteins without a H/L ratio reported for any comparison (see
180 Supp. File 1, accepted sheet). The average of normalized forward and reverse ratios of
181 starvation/control were carried forward for statistical analysis, but only for those with H/L
182 ratios reported for both. These values along with average log_{10} protein intensities were used
183 in Perseus to calculate Significance B values to identify statistical outliers (SigB<0.001) for
184 the three ratios. Data for these shortlisted proteins are summarized in Supp. File 1,

shortlisted sheet. Data is available via ProteomeXchange with identifier PXD024486. Reviewer account details: Username: reviewer pxd024486@ebi.ac.uk Password: ibjQUyjo

Plasmids and site-directed mutagenesis

For all HERPUD1 constructs generated in this study, previously described cDNAs encoding either the full-length or the ΔUBL deletion mutant human HERPUD1, both with a C-terminal FLAG-tag, were used as templates (Sai et al. 2003). pCI-HERPUD1-FLAG and pCI-ΔUBL-FLAG were digested with EcoRI and NotI restriction enzymes to obtain an insert, which was sub-cloned to a lentiviral pLVX-IRES-Puro vector (Takara Bio Inc, CA, USA) containing a puromycin resistance gene. The substitution S59D and S59A were introduced into the pLVX-IRES-FLAG-tagged HERPUD1 vector using the QuikChange II XL direct-mutagenesis kit (Stratagene, cat#200522) and the mutagenesis service of GenScript (Hong Kong, China).

Cell culture and generation of stable cell lines

Maintenance of H4 human neuroglioma cells stably expressing either shRNAs against ATG5 or luciferase genes was performed as previously described (González et al. 2017). HeLa cells were obtained from the American Type Culture Collection (Manassas, VA, USA). HeLa-derived cell lines were cultured in Dulbecco's modified Eagle's medium (DMEM; Thermo Fisher Scientific) supplemented with 10% (vol/vol) heat-inactivated fetal bovine serum (FBS; Thermo Fisher Scientific), and 100 U/ml penicillin/100 mg/ml streptomycin (Thermo Fisher Scientific), in a 5% CO_2 atmosphere at 37ºC. The generation of HeLa stable cell lines expressing all different variants of FLAG-tagged HERPUD1 cloned in the pLVX-IRES-Puro vector were generated by transfection with Lipofectamine 2000 (Invitrogen) according to manufacturer's instructions. After 24 h the cells were selected and maintained with 2 µg/ml of puromycin.

Preparation of protein extracts, Electrophoresis, SDS-PAGE and Western blot analysis

Cells were washed with ice-cold phosphate buffered saline (PBS) and lysed in Radioimmunoprecipitation assay buffer (RIPA lysis buffer) [50 mM Tris-HCl , 150 mM NaCl, 5 mM EDTA, 1% NP-40, 1% sodium deoxycholate, 0.1% SDS, pH 7.4], supplemented with a cocktail of protease inhibitors [416 µM 4-(2-Aminoethyl)benzenesulfonyl fluoride, 0.32 µM Aprotinin, 16 µM Bestatin, 5.6 µM E-64, 8 µM Leupeptin and 6 µM Pepstatin A; Sigma-Aldrich] and phosphatase inhibitors (1 mM NaF, 0,3 mM $Na_2P_2O_7$ and 1 mM Na_3VO_4; Sigma-Aldrich). Cell lysates were collected and lysed for 30 min at 4°C in rotation. Then, extracts were sonicated with ultrasonic power three times on ice with pulses of 2-3 sec at 40 mA using a tip sonicator system. Extracts were further centrifuged for 20 min at 13.000xg at 4°C. The supernatants were collected, and protein concentration was quantified using the BCA assay (ThermoFisher Scientific). The protein extracts were denatured at 65°C for 5 min and analyzed using our previous described methods (González et al. 2017; Bustamante et al. 2020).

Transmission electron microscopy

230 HeLa cells were fixed for 16 h by immersion in 2.5% glutaraldehyde in 0.1 M cacodylate
231 buffer (pH 7.0) at room temperature, and then washed three times with a cacodylate buffer
232 for 2 h. Cells were post-fixed with 1% osmium tetroxide (OsO_4) for 2 h and washed 3 times
233 with double distilled water. Then, the cells were treated with 1% aqueous uranyl for 90 min,
234 and sequentially dehydrated through an acetone battery 50%, 70%, 95%, and 100% for 20
235 min each. Cells were pre-embedded in epon/acetone 1:1 overnight and then in pure epon for
236 4 h. Finally, cells were embedded in fresh resin and polymerized in an oven at 60°C for 48 h.
237 Ultrafine sections (80 nm) were obtained using an ultramicrotome Leica Ultracut R. The
238 sections were incubated with 4% uranyl acetate in methanol for 2 min and lead citrate for 5
239 min. The grids were visualized using a Philips Tecnai 12 electron microscope (Eindhoven,
240 The Netherlands) at 80 kV. This work was performed in the Advanced Microscopy Facility of
241 the Faculty of Biological Sciences at Pontificia Universidad Católica de Chile.

242 **Fluorescence microscopy, data acquisition and quantification**

243 Cells grown on glass coverslips were washed with PBS-Ca^{2+}/Mg^{2+} and then fixed,
244 permeabilized and stained using our published protocols (Bustamante et al. 2020; Cavieres
245 et al. 2020). The images were acquired using a TCS SP8 laser-scanning confocal
246 microscope (Leica Microsystems, Wetzlar, Germany) equipped with a 63× oil immersion
247 objective (1.4 NA), photomultipliers (PMT), hybrid detectors (HyD) system using 405 nm,
248 488 nm, 561 nm and 643 nm laser lines for excitation running the LASX Leica software. For
249 image quantification, 16-bit (1024x1024) images were acquired under identical settings
250 avoiding signal saturation. Cell and nucleus area measurements were performed by using
251 ICY software (Quantitative Image Analysis Unit, Institut Pasteur,
252 http://icy.bioimageanalysis.org/). A pipeline was created to completely automate image
253 analysis by using the following sequential plugins: active contours (cell segmentation), hk-
254 means (threshold detection), wavelet spot detector (spot detection) and studio
255 (colocalization). Total Fluorescence Integrated intensity measurement was performed by
256 using ImageJ (FIJI) (Schindelin et al. 2012). The number of dots (lysosomes) was performed
257 by using the LOG detector algorithm available on the TrackMate plugin (FIJI). For live cell
258 imaging assays, HeLa cells were grown in glass bottom culture dishes (MatTek Corporation,
259 Ashland, MA, USA) and labeled with the following Invitrogen probes: ER-Tracker™ Blue-
260 White DPX (E12353), LysoTracker™ Red DND-99 (L7528, Invitrogen) and Magic-red
261 (Immunochemistry Technologies, LLC) according to the manufacturer's protocol. Before
262 image acquisition, culture medium was replaced with phenol red-free DMEM supplemented
263 with HEPES (10 mM, pH 7.4), and images were acquired with the 63x oil immersion
264 objective (1.4 NA) of the TCS SP8 laser-scanning confocal microscope, running the Leica
265 Application Suite LAS X software, coupled to a controlled temperature chamber (UNO-temp
266 controller, OKOLAB) acquiring 16-bit images at 37ºC (488 laser for excitation; HyD: 510–550
267 nm; 1024 × 1024 pixels; frame average 2). For volume analysis, z-stack (0.3 □m z-interval,
268 1024x1024, 180 □m pixel size) images were quantified using 3D analysis plugin by using
269 ICY software. Total Fluorescence Integrated intensity and dots number were measured
270 using ImageJ.
271
272 **RNA isolation and RT-PCR analysis**
273
274 Total RNA extraction from HeLa cells, oligo-dT and MMLV reverse transcriptase and
275 quantitative reverse transcription PCR of the cDNA template (RT-PCR) was carried out as

276 previously described (Bustamante et al. 2020). The specific primer pairs used for
277 CYCLOPHILIN-A, CYCA (NM_001300981.2) and XBP1 (NM_001079539.2) were the
278 following: **CYCA-F** TCGAGTTGTCCACAGTCAGC, **CYCA-R** TTCATCTGCACTGCCAAGAC, **XBP1-**
279 **F** CGCTTGGGGATGGATGCCCTG and **XBP1-R** CCTGCACCTGCTGCGGACT.
280
281 **Cell viability assays**
282
283 Exponentially growing cells stably expressing either FLAG-tagged HERPUD1-WT or
284 HERPUD1-S59D were trypsinized and seeded at 20,000 cells per well in 96-well microplates
285 and allowed to attach for 6 h at 37°C and 5% CO_2. Then, cells were incubated with CDDP in
286 serial dilutions from 1 mM to 1 μM in 2% FBS medium and were incubated for 24 h at 37°C
287 and 5% CO_2. After drug incubation, the IC50 was obtained using the Sulforhodamine B
288 (SRB) cell cytotoxicity assay (Blois, Smith, and Josephson 2011). Briefly, cells were fixed
289 (10% trichloroacetic acid, 4°C, 1 h), water washed, dried and stained (0.4% SRB v/v in 0.1%
290 acetic acid, 1 h at RT), and then washed four times (1% acetic acid). Dissolved SRB (10 mM
291 Tris-base, pH 10) was quantified (564 nm, Synergy HT BioTek reader). CDDP treatments
292 were done in quadruplicate in at least three independent experiments. The IC50 values
293 associated with the cytotoxic effects of CDDP were calculated using GraphPad Prism
294 software (version 8.2; GraphPad Software, San Diego, CA, USA) using non-linear
295 regression model and dose-response equations (log(inhibitor) vs. normalized response).
296 After drug incubation, apoptotic cells were analyzed with the commercial kit Vybrant
297 Apoptosis Pacific Blue-annexin V (cat#A35122, Invitrogen) using the protocol provided by
298 the manufacturer. Briefly, cells stably expressing either FLAG-tagged HERPUD1-WT or
299 HERPUD1-S59D were treated with 10 μM CDDP for 24 h. Cells were harvested and
300 centrifuged at 800 x g for 5 min at room temperature and washed with cold PBS 1X. Cells
301 were re-centrifuged, and the pellet resuspended in 100 μL annexin-binding buffer. Then, 5
302 μL of the annexin V conjugate was added to the cell suspension and incubated for 15 min at
303 room temperature. After, 400 μL of annexin-binding buffer was added, gently mixed, and
304 maintained on ice for later analysis in a BD FACSCanto II flow cytometer (Flow Cytometer
305 Facility of Cell 4 Cell, Santiago, Chile), with a previous incubation with 3 μL of 7-Amino-
306 Actinomycin D (7AAD) to exclude non-viable cells (included in the kit).
307

308 **Densitometric Quantification and Statistical Analysis**

309 The amount of immunoblot signal was estimated using Image J software version 1.48v
310 (Wayne Rasband, NIH, http://imagej.nih.gov). For each condition, protein bands were
311 quantified from at least three independent experiments in order to ensure adequate
312 statistical power. Data analysis was performed using Microsoft Excel 2013 for Windows
313 (Redmond, WA, USA) or GraphPad Prism 6. Results are represented in graphs depicting the
314 mean ± standard deviation. Statistical significance of data comparisons from two groups
315 comparisons was determined with two-tailed unpaired Student's T-test for parametric data.
316 Values of $P < 0.05$ (*), $P < 0.01$ (**), $P < 0.001$ (***) were regarded as statistically significant
317 and are indicated in the figures.
318
319 **Acknowledgments:** We thank the generous donation of pCI-HERPUD1-Flag and pCI-
320 HERPUD1-ΔUBL-Flag by Doctor Koichi Kokame from National Cerebral and Cardiovascular

Center, Japan. Additionally, we thank Dr. Lavandero and Dr. Quiroga for the critical discussion of the manuscript.

Funding: This research was funded by Fondo Nacional de Desarrollo Científico y Tecnológico of Chile (FONDECYT; http://www.conicyt.cl/fondecyt) No. 1190928 to MV-G, No. 1171649 to P.V.B. & No. 11150532 to A.R.F.; Associative Investigation Program (PIA; https://www.conicyt.cl/pia) including No. ACT-172066 to P.V.B. & No. AFB-170005 to P.V.B.; Academy Insertion Program (PAI; http://www.conicyt.cl/pai) No. 79150075 to A.R.F.; Fondo de Equipamiento Científico y Tecnológico of Chile (FONDEQUIP; http://www.conicyt.cl/fondequip) No. EQM150118 to P.V.B.; Cooperation International Programme (CONICYT-RCUK; https://www.conicyt.cl/pci) No. DPI20140068 to P.V.B.

Statement of interest: The authors declare that there is no conflict of interest.

Competing interest: The authors declare that they have no competing interests.

Data availability statement: All the original data supporting the results is available.

RESULTS

HERPUD1 is a regulator of autophagy under the control of its UBL domain.

Previous reports have demonstrated a close interplay between autophagy and the Ubiquitin-Proteasome System (Bustamante et al. 2018), however, to date, few proteasomal substrates are known as modulators of autophagy (Jia and Bonifacino 2019; Guarascio et al. 2020; Thayer et al. 2020). To search for potential novel candidates that could be downregulated by the proteasome in order to activate autophagy, we performed a SILAC-based proteomic study to quantitatively determine the proteome of H4 neuroglioma cells under basal and induced autophagy by EBSS starvation conditions. To eliminate all proteins downregulated because of autophagy activation, we compared the proteome of H4 cells where autophagy is inhibited by stable depletion of ATG5 by shRNA-mediated knockdown (shATG5) respect to control H4 cells expressing an shRNA against the luciferase gene (shLuc), both cell lines previously characterized (González et al. 2017; Tapia et al. 2019) (Fig. 1A). ATG5 protein is part of a complex with ATG12 and ATG16L that controls an essential step in the autophagosome formation (Walczak and Martens 2013). Silencing of ATG5 causes a strong inhibition in LC3B-positive autophagosomes, a phenotype also previously confirmed in our H4 cell lines (González et al. 2017). Among all the proteins downregulated by EBSS starvation, we found that in both H4 cell lines, shLuc (Fig. 1B) and shATG5 (Fig. 1C) the most significantly downregulated protein was HERPUD1, a protein originally identified as a homocysteine-inducible gene, that is also upregulated by endoplasmic reticulum (ER) stress (K. Kokame et al. 2000; Koichi Kokame, Kato, and Miyata 2001). Importantly, HERPUD1 is an ER-stress membrane protein whose levels under non-stressful conditions are low due to proteasome degradation (K. Kokame et al. 2000; Sai et al. 2003). Indeed, pharmacological inhibition of the proteasome leads to a rapid increase of HERPUD1 levels (Sai et al. 2003; Miura et al. 2010). In addition to HERPUD1, we found several other proteins significantly down- or up-regulated by EBSS treatment (Fig. 1D). However, while some proteins were down- or up-regulated by EBSS treatment in both, shLuc and shATG5 stable expressing cell lines (Fig. 1D, red dots), many other hits were only down or up-regulated dependent on

371 ATG5 protein expression (Fig. 1D, purple dots). The complete list of proteins that responded
372 significantly to EBSS treatment in both cell lines is shown in Suppl. Fig 1. Here, we focus on
373 the characterization of HERPUD1, the hit with the highest score of downregulation in both
374 cell lines, working with the hypothesis that its reduction by EBSS treatment could be
375 indicative of its role as negative regulator of autophagy activity. Previous studies had shown
376 that silencing HERPUD1 triggers the autophagic flux (Quiroga et al. 2013). Therefore, in this
377 study, and considering that HERPUD1 levels are increased under ER stress, we study the
378 cellular consequences of HERPUD1 stability on autophagy function. HERPUD1 is an
379 integral membrane protein with both termini facing the cytoplasm, with the ubiquitin-like
380 domain (UBL) located in its N-terminus (Fig. 2A; UBL: purple color, left side). Here, we
381 cloned full-length HERPUD1 into the pLVX-IRES-Puro vector with a FLAG-tagged in its C-
382 terminal end (Fig. 2A; FLAG: green color) designed as HERPUD1-WT. In addition, we
383 cloned a FLAG-tagged HERPUD1 version lacking the residues between Val^{10}-Cys^{86}
384 designed as HERPUD1-ΔUBL (Fig. 2A; right side), as previously reported (Sai et al. 2003).
385 Further, we generated puromycin-resistant HeLa cells stably expressing either HERPUD1-
386 WT or HERPUD1-ΔUBL, considering that previous characterization of HERPUD1 in HeLa
387 cells was done only by transient transfection (Sai et al. 2003). Western blot analysis using
388 anti-HERPUD1, and anti-FLAG antibodies showed that the levels of HERPUD1-ΔUBL were
389 higher than the levels induced by the overexpression of HERPUD1-WT (Fig. 2B, lane 3 and
390 lane 5). In addition, western blot analysis with an anti-HERPUD1 antibody confirmed
391 HERPUD1 is expressed in low levels under non-stressful conditions (Fig. 2B, lane 1). The
392 UBL is a domain that resembles ubiquitin in terms of their primary sequence and three-
393 dimensional structure, considered a general interaction motif with the proteasome
394 particularly with the 19S regulatory particle of the 26S proteasome (R. Hartmann-Petersen
395 and Gordon 2004). Interestingly, it has been previously shown that deletion of UBL in
396 HERPUD1 abolishes its proteasomal degradation (Sai et al. 2003). To confirm this, we
397 treated the cells during 4 h with 20 μM MG132, a potent blocker of the proteasome activity
398 (Tsubuki et al. 1996; D. H. Lee 1998). As expected, we observed that this treatment caused
399 an increase in the levels of overexpressed HERPUD1-WT (Fig. 2B, lane 3 and 4). Similarly,
400 we observed a slight increase in the levels of endogenous HERPUD1 (Fig. 2B, lane 1 and
401 2). In contrast, HERPUD1-ΔUBL did not respond to this treatment, observing similar levels in
402 the absence or presence of MG132 (Fig. 2B, lane 5 and 6). Together, these results
403 confirmed HERPUD1-ΔUBL is a tool to explore the effect of HERPUD1 stability on
404 autophagy.
405
406 Therefore, we investigated the effect of HERPUD1-ΔUBL stable expression by analyzing the
407 subcellular distribution of the microtubule-associated protein 1 light chain 3B (LC3B), a
408 classical marker of autophagy, from here referred for simplicity as LC3 (Tanida, Ueno, and
409 Kominami 2008). Immunofluorescence analysis of LC3 in cells expressing HERPUD1-WT
410 showed basal autophagy represented by LC3-positive membrane dots that correspond to
411 autophagosomes decorated with lipidated LC3 (LC3-II) (Fig. 3A; left, control). In comparison,
412 we noticed that HERPUD1-ΔUBL cells showed a slight decrease in the number of
413 autophagosomes which was accompanied with a higher LC3 cytosolic distribution (LC3-I)
414 (Fig. 3A; right, control). Because autophagosomes are constantly forming autolysosomes
415 through the fusion with acidic lysosomes for degradation, we tested the effect of BafA1, a
416 drug that raises the lysosomal pH resulting in the perturbation of the autophagic flux
417 (González et al. 2017). As expected, treatment of HERPUD1-WT cells with BafA1 showed a
418 higher number of autophagosomes (Fig. 3A, left, BafA1). In contrast, this treatment in

419 HERPUD1-ΔUBL cells showed fewer numbers of autophagosomes compared to HERPUD1-
420 WT cells (Fig. 3A, right, BafA1). Furthermore, we biochemically validated these results
421 performing western blot analysis of endogenous LC3 (Fig. 3B). We found that under basal
422 conditions overexpression of HERPUD1-ΔUBL caused an increase in LC3-I levels, in
423 comparison to HERPUD1-WT (Fig. 3B, lane 1 and 2). In agreement with this observation,
424 HERPUD1-ΔUBL cells showed a significant reduction in the LC3-II/LC3-I ratio (0.47 ± 0.22),
425 respect to control cells (1.00 ± 0.05) (Fig. 3C). A similar finding was observed in the
426 presence of BafA1 treatment, observing in HERPUD1-ΔUBL cells a significant decrease in
427 the ratio LC3-II/LC3-I (0.94 ± 0.37), respect control cells (3.01 ± 0.78) (Fig. 3B, lane 3 and
428 4). Importantly, similar findings were obtained under induced autophagy by EBSS starvation
429 medium (Suppl. Fig. 2). We observed that the LC3-II/LC3-I ratio in HERPUD1-ΔUBL cells in
430 the presence of EBSS plus BafA1 was diminished with respect HERPUD1-WT cells (Suppl.
431 Fig. 2A, line 5 and 6 and Suppl. Fig. 2B). Altogether, these findings strongly indicate that
432 increased stability of HERPUD1 plays a negative effect on autophagy.
433
434 ***Increased stability of HERPUD1 by the deletion of its UBL domain triggers expansion***
435 ***of the ER organized in stacked tubules and crystalloid ER-like structures in the***
436 ***absence of ER stress.***
437
438 Because previous reports have shown that defective autophagy leads to ER expansion (Ou
439 et al. 1995; Jung et al. 2008) we investigated whether HERPUD1 stability could be linked
440 with ER remodeling. In contrast to previous studies where only transient expression of
441 HERPUD1-ΔUBL was characterized (Sai et al. 2003), we investigated the subcellular
442 distribution of FLAG-tagged HERPUD1-ΔUBL but in stable HeLa cell lines, in comparison
443 with its wild type version. Immunofluorescence analysis with an anti-FLAG antibody showed
444 a stronger signal for HERPUD1 in the absence of its UBL domain (Fig. 4A, FLAG, lower left
445 panel) in comparison to HERPUD1-WT (Fig. 4A, upper left panel). A similar result was also
446 observed with an anti-HERPUD1 antibody (Suppl. Fig. 3A). To unveil if this phenotype was
447 affecting the ER in general, we analyzed by immunofluorescence the distribution of
448 endogenous ER proteins markers. First, we tested endogenous CALNEXIN, an ER
449 membrane resident protein that acts as a molecular chaperone of glycoproteins (Ou et al.
450 1995) and GRP94, an ER resident membrane protein of the Heat-Shock Protein (HSP) 90
451 family (Marzec, Eletto, and Argon 2012). We found profound changes in the distribution of
452 both proteins showing a similar pattern to anti-FLAG in HERPUD1-ΔUBL cells (Fig. 4A,
453 CALNEXIN and GRP94, lower panel), compared to HERPUD1-WT where a characteristic
454 ER pattern is observed. Indeed, HERPUD1-ΔUBL shows a nice colocalization with
455 CALNEXIN and GRP94 (Fig. 4A, lower merge). In addition, and to exclude the possibility
456 that this phenotype was specific to CALNEXIN and GRP94, we analyzed the ER pattern
457 using an ER-tracker probe in live cells, observing clear changes in the morphology of the ER
458 respect to HERPUD1-WT (Suppl. Fig. 3B). We noticed that in comparison to HERPUD1-
459 ΔUBL, HERPUD1-WT did not show a high colocalization with CALNEXIN and GRP94 (Fig.
460 4A, upper merge), which can be explained by the low levels of HERPUD1-WT expression
461 due to its constant degradation by the proteasome under basal conditions (Sai et al. 2003).
462 In this regard, localization of HERPUD1 at the ER has been well documented (K. Kokame et
463 al. 2000). Whereas HERPUD1-ΔUBL did not cause an increase in the levels of CALNEXIN
464 and GRP94 measured by Western blot analysis (Suppl. Fig. 3C y 3D), we concluded that
465 HERPUD1 stability by the deletion of its UBL domain causes an ER-like expansion
466 phenomena that does not involve the increase in the levels of CALNEXIN and GRP94.

467 HERPUD1 is known to be upregulated under ER stress, a condition reported to cause ER
468 membrane expansion to alleviate this condition (Schuck et al. 2009). Therefore, we studied
469 whether HERPUD1-ΔUBL could be causing ER proliferation. To assess this, we performed
470 immunofluorescence analysis with an anti-GRP94 antibody. Interestingly, we observed that
471 HERPUD1-ΔUBL expressing cells present a large and dense ER network extending
472 throughout the entire cytoplasm including the periphery of the cell, compared to the less
473 extended ER network observed in HERPUD1-WT cells (Fig. 4B, left and right panel). To gain
474 a more comprehensive understanding of the ER differences between HERPUD1-WT and
475 HERPUD1-ΔUBL expressing cells, we measured the ER volume using 3D images at high
476 magnification taken with a z-interval of 0.3 µm followed by a z-stack maximum intensity
477 projection. For visualization, we analyzed the distribution of GRP94 in the whole cell using a
478 heat map gradient ranging from non-intensity (black color) to the higher intensity (red color)
479 (Fig. 4B, left and right panel). This analysis confirmed HERPUD1-ΔUBL increases the
480 volume of the ER and the expansion of this organelle, compared to the expression of
481 HERPUD1-WT. Indeed, quantitative analysis showed a significant increase in the ER
482 volume with the expression of HERPUD1-ΔUBL (2361 ± 967), compared to HERPUD1-WT
483 (1700 ± 689) (Fig. 4C). The ER morphological changes observed by confocal microscopy
484 prompted us to perform ultra-structural analysis by transmission electron microscopy (TEM).
485 While cells expressing HERPUD1-WT showed the common ER cytoplasmic structures (Fig.
486 4D left panel [ER]), unexpectedly HERPUD1-ΔUBL showed a high number of staked tubular
487 ER structures oriented in a hexagonal spatial distribution (Fig. 4D center panel [ER]). Others
488 have referred to these structures as energetically stable structures formed by a remarkable
489 proliferation of smooth ER, resembling crystalloid structures of ER (Chin et al. 1982;
490 Anderson, Orci, and Brown 1983; Borgese, Francolini, and Snapp 2006), which in
491 appearance can be compared with "honeycomb like-structures" (Fig. 4D center panel [ER]).
492 Additionally, a higher magnification (Fig. 4D, right panel), confirmed the ER contained in the
493 crystalloid structure corresponds to smooth ER evidenced by the absence of attached
494 ribosome structures.
495
496 To gain insights whether the ER proliferation triggered by the expression of HERPUD1-
497 ΔUBL was the result of an ER stress response, we studied X-box binding protein 1 (XBP1)
498 as a reporter of ER stress and the unfolded protein response (UPR). First, we analyzed by
499 RT-PCR the XBP1 mRNA processing, from the unspliced inactive XBP1 mRNA (u*XBP1*)
500 form to the spliced active XBP1 mRNA (s*XBP1*) form (Fig. 5A), which is considered a
501 hallmark of the UPR response (Yoshida et al. 2001). RT-PCR analysis of mRNA from HeLa
502 WT untreated cells showed a single band as expected (Fig. 5A, lane 1). The same analysis
503 including tunicamycin (Tun) (inhibitor of N-linked glycosylation (Heifetz, Keenan, and Elbein
504 1979) and thapsigargin (Tg) (blocker of ER Ca2+ import (Thastrup et al. 1990)) as positive
505 inducers of ER stress, produced the appearance of two bands in HeLa-WT cells, indicating
506 the s*XBP1* form in response to ER stress (Fig. 5A, lane 2 and 3). In contrast, a stable
507 expression of either HERPUD1-WT or HERPUD1-ΔUBL showed no detection of s*XBP1,*
508 observing only the expression of the u*XBP1* form (Fig. 5A, lane 4 and 5), similar to control
509 HeLa WT untreated cells (Fig. 5A, lane 1). Analysis of PCR bands relative to *CYCLOPHILIN*
510 *A (CYC-A)* as a housekeeping control showed no difference between cells expressing either
511 HERPUD1-WT or HERPUD1-ΔUBL proteins (Fig. 5A, lane 4 and 5). Similar findings were
512 observed by western blot analysis (Fig. 5B). s*XBP1* is rapidly translated to a highly active
513 transcription factor, known as XBP1, responsible for the upregulation of a variety of UPR
514 genes (Yoshida et al. 2001). To examine the significance of the UBL domain of HERPUD1 in

515 the response to ER stress induction, HERPUD1-WT cells and HERPUD1-ΔUBL cells were
516 treated with 2 μM Tg for 2, 4 and 6 h and we performed western blot analysis for XBP1
517 detection. We observed XBP1 protein was almost undetectable in both cell lines in the
518 absence of a stressor (Fig. 5B, lane 1 and 5). In contrast, we observed a robust induction of
519 XBP1 in both cell lines upon treatment for 2, 4 and 6 h with 2 μM Tg, observing similar XBP1
520 expression levels after 6 h of treatment in both cell lines (Fig. 5B, lane 4 and 8). Quantitative
521 analysis confirmed this conclusion, observing no significant differences between HERPUD1
522 WT (58.99 ± 9.18) and HERPUD1-ΔUBL (59.59 ± 17.49) expressing cells (Fig. 5C). In
523 addition to XBP1, we tested by western blot analysis the ER resident transmembrane protein
524 PERK, a kinase that undergoes hyperphosphorylation in response to ER stress shown as a
525 shift in its mobility during SDS-polyacrylamide gel electrophoresis (Bertolotti et al. 2000).
526 This kinase mediates the attenuation of the global translation by the phosphorylation of
527 eIF2α (Bertolotti et al. 2000; Harding, Zhang, et al. 2000). In contrast to its differential
528 electrophoretic migration with Tun and Tg (Suppl. Fig. 4, lane 2 and 3), no changes in PERK
529 migration were observed in HERPUD1-WT or HERPUD1-ΔUBL cells (Suppl Fig. 4, lane 4
530 and 5). Analysis of the activating transcription factor 4 (ATF4), a protein highly expressed
531 upon UPR response (Harding, Novoa, et al. 2000) showed again no changes in ATF4 levels
532 in either cell line (Suppl. Fig. 4, lane 4 and 5). In contrast, a robust detection of ATF4 was
533 found upon the addition of Tun and Tg (Suppl. Fig. 4, lane 2 and 3). Altogether, our findings
534 strongly indicate that the maintenance of the ER expansion triggered by HERPUD1 stability
535 is not the consequence of ER stress.
536
537 ***Increased HERPUD1 stability by the deletion of its UBL domain leads to a remarkable***
538 ***increase in lysosomal number and function***
539
540 ER proliferation that excludes ribosomes is able to regulate ER contacts with lysosomes
541 (Friedman et al. 2013; C. A. Lee and Blackstone 2020). Lysosomes are an important
542 catabolic organelle of eukaryotic cells, containing a diverse repertoire of acidic hydrolases
543 (luminal pH of 4.5–5.0) that can digest macromolecules such as sugars, lipids and proteins
544 and even entire organelles (H. Xu and Ren 2015). We asked whether expanded ER by
545 increased HERPUD1 stability could have an impact on endolysosomal organelles. To
546 visualize these compartments, HERPUD1-WT and HERPUD1-ΔUBL expressing HeLa cells
547 were stained with an antibody against the endogenous lysosomal-associated membrane
548 protein 1 (LAMP1), a membrane protein found on late endosomes and lysosomes (Griffiths
549 et al. 1988). Unexpectedly, we observed a robust increase in LAMP1 positive structures
550 located around the entire cytoplasm (Fig. 6A). In agreement with this finding, quantification
551 analysis showed a significant increase in the number of LAMP1 positive structures in
552 HERPUD1-ΔUBL (88.72 ± 16.77) respect to control cells (69.03 ± 13.79) (Fig.6B). To
553 determine if the increase in LAMP1 structures corresponded to lysosome organelles, we
554 performed co-staining of LAMP1 with CATHEPSIN-D (CAT-D), a luminal hydrolytic
555 lysosomal enzyme (Benes, Vetvicka, and Fusek 2008), observing several LAMP1 positive
556 structures positive to CAT-D (Suppl. Fig 5A, lower merge). In addition, we noticed a
557 significant increase in the integrated fluorescence intensity of CAT-D in HERPUD1-ΔUBL
558 (1.47 ± 0.88), compared to HERPUD1-WT expressing cells (1.00 ± 0.20) (Suppl. Fig 5B).
559 Considering this increase in CAT-D fluorescence we evaluated if HERPUD1-ΔUBL also
560 impacts lysosomal activity, as assessed by measuring lysosomal acidity and activity in live
561 cells. We first measured if HERPUD1 stability affects the range of lysosomal pH, using the

562 pH-sensitive lysosomal dye LysoTracker Red, which accumulates and emits red
563 fluorescence in acidic compartments with pH <6.5 (De Duve et al. 1974; Chou, Paul
564 Krapcho, and Hacker 2001). Then, we measured CATHEPSIN-B activity using the Magic
565 Red assay (Boonacker et al. 2003). As shown in Figure 6C, expression of HERPUD1-ΔUBL
566 causes a significant increase in the number of LysoTracker positive structures (211.95 ±
567 78.90), compared to control cells (117.85 ± 48.97) (Fig. 6C and 6D). Similarly, we found an
568 increase in the number of structures positive to Magic Red fluorescence (Figure 6E). This
569 was confirmed by measuring the integrated fluorescence intensity, which revealed a
570 significant increase of this parameter in HERPUD1-ΔUBL cells (1.56 ± 0.43), compared to
571 control cells (1.00 ± 0.19) (Fig. 6F). Altogether, these findings show that ER expansion
572 triggered by HERPUD1 increased stability is a potent strategy to promote lysosomal
573 function.
574
575 ***The phosphomimetic mutant S59D in the UBL domain promotes HERPUD1 stability***
576 ***mimicking the effects of UBL deletion on the ER and autophagy.***
577
578 Further, we searched for a mechanism that could mimic the phenotype observed by the
579 deletion of UBL on HERPUD1. As shown by the analysis with PyMOL molecular graphics
580 system (Suppl. Fig 6A), the UBL domain of HERPUD1 (PDB 1WGD; green color) resembles
581 UBIQUITIN (PDB 2MSG; purple color) in terms of their three-dimensional structure.
582 UBIQUITIN as well as UBL domains are known targets of phosphorylation under cellular
583 stress (Kondapalli et al. 2012; Swaney, Rodríguez-Mias, and Villén 2015; Sauvé et al. 2018).
584 In fact, oxidative stress promotes phosphorylation of UBIQUITIN at Ser65 causing the
585 accumulation of ubiquitylated proteins due to a reduction in global protein turnover rates
586 (Koyano et al. 2014; Swaney, Rodríguez-Mias, and Villén 2015). In the same line, it is known
587 that the UBL domain on PARKIN is phosphorylated by PINK1, and is responsible for the
588 activation of its E3 ubiquitin-ligase activity (Sauvé et al. 2018), both essential players of
589 mitochondria quality control by mitophagy (Jin and Youle 2012). Thereby, we searched for
590 Ser residues as possible candidates of phosphorylation in the UBL domain of HERPUD1
591 using the KinasePhos2.0 web tool. Five residues were predicted in position Ser16, Ser27,
592 Ser33, Ser59 and Ser90 (Suppl. Fig 6B, Ser residues in red color). For all these five Ser
593 residues, we generated phosphoinert (substitutions to alanine) and phosphomimetic
594 (substitutions to aspartic acid) mutant versions. Stably transfected HeLa cells were
595 generated for each mutant. Among all mutations tested, the substitution S59D, but not the
596 S59A, showed the strongest increase in HERPUD1 signal, as is shown by
597 immunofluorescence with an anti-FLAG antibody (Fig. 7A and 7B). Importantly, we found
598 that the phosphomimetic S59D mutant presents an ER pattern very similar to HERPUD1-
599 ΔUBL cells, confirmed by the co-staining with GRP94 (Fig. 7A, right panel merge). In
600 contrast, no changes were observed with the phosphoinert S59A mutant, showing a similar
601 phenotype than HERPUD1-WT (Fig. 7A and 7B). Thus, further characterization included the
602 comparison between HERPUD1-WT and HERPUD1-S59D. In addition, under basal
603 conditions western blot analysis using anti-HERPUD1 and anti-FLAG antibodies showed
604 higher levels of HERPUD1-S59D (40.09 ± 5.31) compared to either HERPUD1-WT (1.00 ±
605 0.53) or HERPUD1-S59A (2.88 ±1.76) (Fig. 7C, lane 5 compared to lane 1 and 3 and Fig.
606 7D). We also measured the levels of these versions upon treatment for 4 h with 20 mM
607 MG132, which is a proteasomal inhibitor, known to abolish HERPUD1 proteasomal
608 degradation (Yan et al. 2014). As expected, MG132 treatment caused a significant increase
609 in HERPUD1-WT (16.55 ± 7.13) (Fig. 7C, lane 1 compared to lane 2 and Fig. 7D). A similar

610 result was obtained with HERPUD1-S59A (20.36 ± 9.65) (Fig. 7C, lane 3 compared to lane 4
611 and Fig. 7D). In contrast, we observed non-significant differences in the levels of HERPUD1-
612 S59D in the absence (40.09 ± 5.31) or presence of MG132 (47.17 ± 11.74) (Fig. 7C, lane 5
613 and 6 and Fig. 7D). Further, and based on the negative impact of HERPUD1 stability on
614 autophagy by the deletion of its UBL domain, we next investigated if the stability of
615 HERPUD1-S59D could have a similar outcome. Biochemically, we found that HERPUD1-
616 S59D cells have a significant reduction in the LC3-II/LC3-I ratio (0.66 ± 0.02), in comparison
617 to HERPUD1-WT (1.00 ± 0.18) (Fig. 7E and 7F). This result was corroborated by
618 immunofluorescence analysis of LC3 in the absence or presence of BafA1 showing that
619 HERPUD1-S59D cells present a lesser number of autophagosomes, compared to
620 HERPUD1-WT (Suppl. Fig. 7). Moreover, in agreement with previous reports indicating that
621 a reduction in autophagy enhances ER expansion and cell size (Khaminets et al. 2015;
622 Miettinen and Björklund 2015), we noticed that HERPUD1-S59D cells were significantly
623 larger in size (2.52 ± 0.98), compared to HERPUD1-WT (1.00 ± 0.4) and HERPUD1-S59A
624 cells (0.88 ± 0.29) (Fig. 7A and Suppl. Fig. 8A). Importantly, cell size quantification showed
625 HERPUD1-ΔUBL were also larger in size (1.36 ± 0.64) than HERPUD1-WT (1.00 ± 0.4), but
626 smaller than HERPUD1-S59D (2.52 ± 0.98) (Suppl. Fig. 8A). In addition, because nuclei size
627 remains proportional to the cell size in a wide range of genetic backgrounds and growth
628 conditions (Huber and Gerace 2007), we studied the nuclei size in all cell lines. Surprisingly,
629 nuclei size in HERPUD1-S59D cells were significantly larger (1.74 ± 0.72) in comparison to
630 all tested cell lines; HERPUD1-WT (1.00 ± 0.49), HERPUD1-S59A (1.12 ± 0.47) and
631 HERPUD1-ΔUBL (1.11 ± 0.52) (Suppl. Fig. 8B). Altogether, our findings support the idea
632 that HERPUD1 increased stability might play an important function in cellular plasticity by
633 commanding a program that controls ER expansion with impact in cell and nuclei size. The
634 results with the phosphomimetic version of HERPUD1 opens the alternative of a program
635 activated under the control of phosphorylation.
636
637 ***The phosphomimetic HERPUD1-S59D mutant promotes ER-lysosomal network with***
638 ***impact in stress cell survival***

639 Because of the increase in the number of functional lysosomes under the expression of
640 HERPUD1-ΔUBL, we investigated if HERPUD1-S59D expressing cells could have a similar
641 output. First, we performed immunofluorescence of LAMP1, observing a significant increase
642 in the number of LAMP1 positive structures in HERPUD1-S59D cells (135.28 ± 21.32), in
643 comparison to HERPUD1-WT (69.03 ± 13.79) and HERPUD1-S59A (58.42 ± 14.55) (Supp.
644 Fig. 9A and 9B). Next, analysis with LysoTracker in HERPUD1-S59D cells (183.35 ± 60.05),
645 in comparison to HERPUD1-WT (118.18 ± 51.00) and HERPUD1-S59A (86.13 ± 41.46)
646 confirmed HERPUD1-S59D cells have a significant increase in the number of lysosomes per
647 cell (Suppl. Fig. 9C and 9D). Similar results were obtained with Magic Red where the
648 quantification showed an increase of almost twice the intensity of Magic Red in HERPUD1-
649 S59D cells (2.25 ± 0.32) in comparison with HERPUD1-WT (1.00 ± 0.15) and HERPUD1-
650 S59A (1.02 ± 0.24) (Suppl. Fig 9E and 9F).

651 One important aspect of cellular plasticity is the establishment of a network between the ER
652 and the lysosomes that helps in the constant adaptation to particular cellular needs. In this
653 regard, it is known that the ER forms membrane-contact sites (MCSs) with lysosomes (Valm
654 et al. 2017), acting as a potent spatiotemporal organizer of endolysosomal biology (Neefjes,
655 Jongsma, and Berlin 2017). We hypothesized that the expansion of the ER-lysosomal

656 network should be accompanied by the appearance of MCSs between these two organelles.
657 Therefore, we studied the spatial distribution of the ER and lysosomes upon stability of
658 HERPUD1 with the expression of HERPUD1-ΔUBL and HERPUD1-S59D. For this, multiple
659 confocal images were obtained with CALNEXIN and LAMP1 co-staining by
660 immunofluorescence and analyzed in a super-resolution scale. As expected, we observed
661 that similar to HERPUD1-WT expression, expression of HERPUD1-ΔUBL and HERPUD1-
662 S59D form ER-lysosomes MCSs (Fig. 8 middle panel). MCSs are also shown in a three-
663 dimensional (3D) reconstruction with high magnification (Fig. 8 inset lower panel).
664 Altogether, our findings strongly suggest that expansion of ER by HERPUD1 stability not
665 only promotes the remodeling of the lysosomal network but also the formation of MCSs
666 between these two organelles.

667 ER expansion has been known for decades as a trigger for crystalloid ER (Chin et al. 1982)
668 and ER whorls (Feldman, Swarm, and Becker 1981; Schuck et al. 2009), however only
669 recent studies have proposed this phenomenon could be part of a program necessary to
670 overcome ER stress with impact in stress cell survival (Schuck et al. 2009; F. Xu et al.
671 2021). Moreover, taking in consideration that HERPUD1 stability triggers ER expansion, ER-
672 lysosomal network and MCSs between these two organelles, a protein known to be
673 upregulated under ER stress, we studied the effect of HERPUD1 stability in the cell viability
674 of HeLa cells in response to cisplatin (CDDP). CDDP is the most frequently used
675 chemotherapeutic agent for the treatment of some types of cancers, including cervical
676 cancer in accordance with the model of HeLa cells (Dasari and Bernard Tchounwou 2014).
677 In addition, it is known that alleviation of ER stress attenuates CDDP-induced apoptosis (Wu
678 et al. 2018). Thus, we investigated the resistance to drug-induced cytotoxicity of HERPUD-
679 WT and HERPUD1-S59D cells in response to varying doses of CDDP for 24 h with the
680 Sulforhodamine B (SRB) assay. We found a significant increase in the resistance of
681 HERPUD1-S59D cells in comparison with HERPUD1-WT at 2, 4, 8 and 16 μM of CDDP
682 (Fig. 9A). We corroborated this result measuring apoptosis of these cells in the absence or
683 presence of 10 μM CDDP for 24 h by flow cytometry using Annexin-V staining method. In
684 agreement with the SRB assay, we observed HERPUD1-S59D cells showed less apoptosis
685 compared to HERPUD1-WT cells in response to CDDP treatment (Fig. 9B). These results
686 strongly indicate HERPUD1 stability helps to overcome cisplatin-induced cytotoxicity. In this
687 regard, we propose that this differential response could be mediated by the expansion of the
688 ER/lysosomal network, an aspect that should be investigated in other cancer cell models.

689 **DISCUSSION**

690 Post-translational responses allow cells to respond swiftly to stress conditions with
691 consequences in their proteome composition. Autophagy and the UPS are two closely
692 related pathways that adjust their functions in response to cellular demands in order to
693 maintain cellular homeostasis (Korolchuk, Menzies, and Rubinsztein 2010). During
694 starvation overall protein degradation rises by activation of both autophagy and the UPS
695 (Mizushima, Yoshimori, and Ohsumi 2011; VerPlank et al. 2019). Indeed, before up-
696 regulation of autophagy, efficient synthesis of new proteins is sustained by degradation of
697 preexisting proteins by the proteasome, which shows that the proteasome also plays a
698 crucial role in cell survival after nutritional stress (Vabulas and Hartl 2005). In agreement
699 with this, it is known that the proteasome activity transits from a latent to an activated state
700 (Asano et al. 2015; Collins and Goldberg 2020). However, if UPS activation upon starvation

701 mediates the degradation of specific proteins that could slow-down autophagy is unknown.
702 Downregulation of HERPUD1 upon nutrient starvation in ATG5-depleted cells opens that
703 alternative. In this regard, it has been previously proposed that HERPUD1 depletion up-
704 regulates autophagy (Quiroga et al. 2013) and the degradation of cytosolic protein
705 aggregates (Miura et al. 2010). These findings support the idea that basal levels of
706 HERPUD1 could act as a break in the activation of basal autophagy.

707 Under ER stress, HERPUD1 is upregulated even faster than ER chaperones (K. Kokame et
708 al. 2000; Bergmann et al. 2018), where it participates in Endoplasmic Reticulum-Associated
709 Degradation (ERAD) (Schulze et al. 2005). HERPUD1 facilitates the assembly of the HRD1
710 complex, also known as the retrotranslocon, key in the retrotranslocation of unfolded
711 proteins from the ER to the cytosol for proteasomal degradation upon demand (Leitman et
712 al. 2014; Schulz et al. 2017). However, the function of HERPUD1 in the absence of ER
713 stress is less understood. Here, we propose HERPUD1 acts as a negative regulator of
714 autophagy controlled by its proteasome dependent stability, a mechanism that could operate
715 in the absence of ER stress under the control of phosphorylation of its UBL domain.

716 One interesting aspect of HERPUD1 is the UBL domain present in its N-terminus region. In
717 general, UBL-containing proteins share the ability to interact with the 19S regulatory particle
718 of the 26S proteasome promoting its activation (Rasmus Hartmann-Petersen and Gordon
719 2004; Yu and Matouschek 2017; Collins and Goldberg 2020). The UBL domain itself can
720 stimulate multiple proteasome activities in a similar fashion to ubiquitin chains (H. T. Kim and
721 Goldberg 2018; Collins and Goldberg 2020). However, unlike ubiquitin and its homologous
722 (e.g., SUMO and Nedd8), UBL-containing proteins cannot be conjugated to other proteins.
723 The human genome encodes over 60 UBL-containing proteins, where 15 of them have been
724 studied in their ability to bind and regulate proteasome activity (Collins and Goldberg 2020).
725 HERPUD1 is one member of this group, however its role as a positive modulator of the
726 proteasomal activity remains uncharacterized. Moreover, because UBL-containing proteins
727 can stimulate proteasome activity (H. T. Kim and Goldberg 2018; Collins and Goldberg
728 2020), it would be interesting to explore the effect of HERPUD1-ΔUBL and HERPUD1-S59D
729 on the activity of the proteasome under normal and starvation conditions.

730 In addition, recent findings show UBL-containing proteins can also play a regulatory role in
731 autophagy, such as USP14 (E. Kim et al. 2018), NUB1 (Guarascio et al. 2020), Elongin B
732 (Antonioli et al. 2016), UHRF1 (Shi et al. 2020), OASL (Batista-Silva et al. 2018), BAT3
733 (Sebti et al. 2014) and UBQLN (Rothenberg et al. 2010; Şentürk et al. 2019; Yang and
734 Klionsky 2020). Our findings show that the stabilization of HERPUD1 by lacking its UBL
735 domain causes a reduction in LC3-II/LC3-I ratio, which positions HERPUD1 as a member of
736 this growing list of UBL-containing proteins that function as regulators of autophagy.
737 However, how HERPUD1 stability mediates the reduction in LC3-II/LC3-I ratio needs further
738 studies. One aspect to be explored is the finding that HERPUD1 interacts with UBQLN (T. Y.
739 Kim et al. 2008). UBQLN is a cytosolic protein, that in addition to HERPUD1, interacts with
740 LC3 and ubiquitinated cargos in autophagosomes (Rothenberg et al. 2010). Furthermore, it
741 is known that silencing UBQLN leads to a reduction in the lipidation of LC3-I to LC3-II that
742 correlates with a diminished number of autophagosomes (Rothenberg et al. 2010). Because
743 UBQLN binds HERPUD1 independently of its UBL domain (T. Y. Kim et al. 2008), it is
744 possible that an increase in HERPUD1 stability at the ER could mediate the sequestration of
745 UBQLN in this compartment affecting its function in other membranes such as

746 autophagosomes (Rothenberg et al. 2010). In this regard, it has been previously proposed
747 that recruitment of UBQLN to the ER by HERPUD1 could bring the proteasome and the
748 ubiquitinated substrates to specific microdomains of the ER, which could hypothetically be
749 the step that promotes the ERAD pathway (T. Y. Kim et al. 2008). Because our results show
750 that HERPUD1 stability maintain the ER-lysosomal network, additional work is needed to
751 determine if HERPUD1:UBQLN interaction could play a role in the delivery of substrates to
752 the ER-to-lysosomes-associated degradation (ERLAD) (Fregno et al. 2018; Fregno and
753 Molinari 2019), considering the increase in the lysosomal degradation function. As
754 HERPUD1-S59D mimics the effect on HERPUD1 stability we propose that recruitment of
755 UBQLN at the ER is controlled by phosphorylation of HERPUD1.

756 Ubiquitin and UBL domains are targets of phosphorylation (Kondapalli et al. 2012; Koyano et
757 al. 2014; Wauer et al. 2015). The best-known example is the phosphorylation of the UBL
758 domain of the ubiquitin ligase PARKIN by the Ser/Thr kinase PINK1 on Ser65 (Kondapalli et
759 al. 2012; Koyano et al. 2014). This post-translational modification orchestrates its enzymatic
760 E3 ligase activity (Aguirre et al. 2017), participating in the ubiquitination of mitochondrial
761 proteins during mitophagy. Here, we propose that phosphorylation of the UBL domain in
762 HERPUD1 must affect its noncovalent binding to the proteasome explaining its stability
763 increase, as occurs with HERPUD1-ΔUBL. Further studies are needed to define the
764 physiological triggers of HERPUD1 phosphorylation, and the kinase involved.

765 This study is the first report indicating HERPUD1 stability mediates ER expansion but not as
766 a consequence of ER stress. In this regard, it is well known that the ER expands to alleviate
767 ER stress (Schuck et al. 2009). However, the ER expansion phenomenon is not always
768 homeostatic. ER expansion requires an adequate supply of membrane lipids although the
769 mechanisms that govern ER biogenesis are yet unclear. For example, the ER expands
770 several folds when B lymphocytes differentiate into antibody-secreting plasma cells (Wiest et
771 al. 1990), when hepatocytes increase its P450 detoxification system (Feldman, Swarm, and
772 Becker 1981), in response to Epidermal Growth Factor (EGF) (Caldieri et al. 2017) and
773 statins (Chin et al. 1982). Interestingly, lipid synthesis activation causes expansion of the ER
774 and resistance to ER stress even in cells lacking the UPR, highlighting the physiological
775 importance of ER membrane biogenesis in homeostasis. A future challenge will be to sort
776 out the connection between HERPUD1 and lipid synthesis, a link recently suggested by
777 genomics (Van Der Laan et al. 2018).

778 In this regard, an interesting observation to be considered is that HERPUD1 increased
779 stability mimics the effect of statins in reference to the appearance of a crystalloid ER (Chin
780 et al. 1982). Statins are cholesterol reducing agents acting as blockers of the cholesterol
781 biosynthesis by the inhibition of 3-hydroxy-3-methylglutaryl coenzyme A (HMG-CoA)
782 reductase. Interestingly, statins possess beneficial effects in a variety of human diseases.
783 Importantly, a growing number of studies refer to statins as ER stress reducing agents
784 (Mollazadeh et al. 2018; T. Zhang et al. 2018), modulators of autophagy (Ashrafizadeh et al.
785 2020) and inducers of lysosomal biogenesis (Y. Zhang et al. 2020). However, if statins
786 promote those effects by a mechanism related with HERPUD1 stability is unknown.

787 Expansion of ER by HERPUD1 stability is correlated with a slow-down in autophagy. In
788 agreement with this, it is known that the knockdown of the two major autophagy regulators,
789 ATG5 and BECN1, likewise trigger ER expansion (Khaminets et al. 2015). Moreover, a

790 similar ER expansion is also observed by ER-phagy inhibition, a selective form of autophagy
791 responsible for the degradation of excess ER (Khaminets et al. 2015; Grumati, Dikic, and
792 Stolz 2018). However, studies investigating if the UPR is activated or not in response to
793 inhibition of autophagosomal biogenesis or ER-Phagy dysfunction are still lacking. While the
794 opposite effect has been reported, observing that excessive ER-Phagy results in activation
795 of the UPR response (Liao et al. 2019).

796 Our findings also indicate that ER expansion by HERPUD1 stability is accompanied by an
797 increase in the number of functional lysosomes. Because several studies have indicated that
798 UBL-containing proteins cause a positive modulation of the UPS system we can speculate
799 that HERPUD1-ΔUBL and HERPUD1-S59D could have a negative impact in the proteasome
800 activity. Disturbances in the UPS and autophagy function are known to be compensated by
801 lysosome biogenesis (Jackson and Hewitt 2016). In addition, we have already discussed the
802 possibility that HERPUD1 stability could trigger the recruitment of UBQLN to the ER.
803 Interestingly, it has been recently discovered that UBQLN plays a crucial role in the
804 maintenance of the acidic pH of lysosomes and in a closed interplay with the ER (Şentürk et
805 al. 2019; Yang and Klionsky 2020). Further work is needed to determine if
806 HERPUD1:UBQLN interaction could play a role at this level. Furthermore, based on recent
807 findings (Toulmay and Prinz 2011; Henne 2017), it is necessary to explore if MCSs between
808 ER and lysosomes could play a role in the transfer of lipids to lysosomes to compensate for
809 the massive expansion of the ER under HERPUD1 stability by degradation.

810 Together, our findings highlight novel insights into the possible role of HERPUD1 as a
811 regulator of autophagy and its participation in the maintenance of the ER structure.
812 Moreover, our results suggest that HERPUD1 stabilization promotes the lysosomal function
813 which could promote ER-lysosome intercommunication even in conditions where the UPR is
814 not activated. The mechanism behind this regulation remains to be elucidated, specially the
815 UBL phosphorylation-dependent stabilization of HERPUD1 and its effect on the pathways
816 discussed above. Furthermore, if this regulation has a role in cell pathological conditions it
817 should be analyzed in future studies.

818 ***Figure legends***

819 **Figure 1. SILAC-based proteomic study reveals HERPUD1 as a possible modulator of**
820 **autophagy. (A)**. Design of the SILAC experiment to monitor changes of the cellular
821 proteome of H4 cells during starvation and shRNA-mediated knockdown of ATG5 (shATG5)
822 or shRNA against the luciferase gene (shLuc). 'Reference' mixes of all cell extracts were
823 prepared for light and heavy conditions for 'forward' and 'reverse' SILAC experiments and
824 were mixed 1:1 with individual cell extracts, giving a total of 8 mixes. **(B-C)** Scatter plot
825 comparing 'Forward' and 'Reverse' Log2 Starvation/Normal ratio data for cells shLuc (B) and
826 shATG5 (C). **(D)** Comparison of average Log_2 Starvation/Normal ratios in shLuc (x-axis) and
827 shATG5 (y-axis). Protein outliers under either or both knockdown conditions are colored as
828 indicated.
829

830 **Figure 2. Deletion of UBL domain increases HERPUD1 protein levels. (A)** Schematic
831 representation HERPUD1-WT (left image) and ΔUBL (right image) at the ER membrane,
832 both FLAG-tagged at the carboxyl-terminus (shown in green). The Ubiquitin-Like domain

833 (UBL, amino acids 10-86) are represented in purple. **(B)** HeLa cells untransfected (UT) or
834 stably expressing the WT or ΔUBL versions of HERPUD1 were not treated (lanes 1, 3 and 5)
835 or treated with 20 μM of MG132 for 4 h (lanes 2, 4 and 6). Detergent-soluble protein extracts
836 were analyzed by western blot with anti-HERPUD1 and anti-FLAG antibodies. β-ACTIN was
837 used as loading control. Position of molecular mass markers is indicated on the left.

838 **Figure 3. The stabilization of HERPUD1 by its UBL deletion negatively regulates**
839 **autophagy. (A)** HeLa cells stably expressing HERPUD1-WT-FLAG or HERPUD1-ΔUBL-
840 FLAG were grown in glass coverslips and were treated or not with 100 nM BafA1 for 4 h.
841 Cells were fixed and incubated with an antibody to LC3 followed by incubation with Alexa-
842 488-conjugated donkey anti-rabbit IgG. Stained cells were examined by confocal
843 microscopy. Scale bar 10 μm. **(B)** HeLa cells stably expressing HERPUD1-WT-FLAG or
844 HERPUD1-ΔUBL-FLAG untreated (lanes 1 and 2) or treated with 100 nM BafA1 for 4 h
845 (lanes 3 and 4). Detergent-soluble protein extracts were analyzed by western blot with a
846 rabbit polyclonal antibody against LC3. Monoclonal antibody against β-ACTIN (clone BA3R)
847 was used as loading control. Position of molecular mass markers is indicated on the left. **(C)**
848 Densitometry quantification of LC3-I and LC3-II protein levels from images as those shown
849 in B. Relative levels are expressed as the ratio of LC3-II to LC3-I. Bars represent the mean ±
850 standard deviation. Statistical analysis was performed using two-tailed unpaired Student's t-
851 test (n = 3 ** $p < 0.01$, *** $p < 0.001$)

852 **Figure 4. HERPUD1-ΔUBL stabilization alters the ER morphology. (A)** HeLa cells stably
853 expressing HERPUD1-WT-FLAG or HERPUD1-ΔUBL-FLAG grown in glass coverslips were
854 fixed, permeabilized and triple-labeled with a mouse monoclonal antibody against FLAG,
855 with a rabbit monoclonal antibody against CALNEXIN and with a rat monoclonal antibody
856 against GRP94 followed by incubation with Alexa-488-conjugated donkey anti-rabbit IgG
857 (green channel), Alexa-594-conjugated donkey anti-rat IgG (red channel) and Alexa-647-
858 conjugated donkey anti-mouse IgG (blue channel). Images were acquired using a TCS SP8
859 laser-scanning confocal microscope. The fourth image on each row is the merge of blue,
860 green and red channels; yellow indicates colocalization of the red and green channels, cyan
861 indicates colocalization of the green and blue channels, magenta indicates colocalization of
862 the red and blue channels, and white indicates colocalization of all three channels. Scale
863 bar, 10 μm. **(B)** HeLa cells stably expressing HERPUD1-WT-FLAG or HERPUD1-ΔUBL-
864 FLAG grown in glass coverslips were fixed, permeabilized and labeled with rat monoclonal
865 antibody against GRP94 followed by incubation with Alexa-594-conjugated donkey anti-rat
866 IgG. Stained cells were examined by fluorescence microscopy. Images were acquired using
867 a TCS SP8 laser-scanning confocal microscope. Pseudocolor image was created using all
868 the serial confocal sections of HeLa HERPUD1-WT-FLAG (left image) and HERPUD1-
869 ΔUBL-FLAG (right image). The scale on the right represents the maximum (red) to minimum
870 (black) intensity measured for GPR94. **(C)** Quantification of ER-volume obtained from serial
871 image reconstruction (z-stack 0.3 μm z-interval, 1024x1024, 180 μm pixel size). Volume is
872 depicted in a scatter plot, open circles represent HeLa HERPUD1-WT-FLAG (n=79) and
873 open squares HERPUD1-ΔUBL-FLAG (n=72). Statistical analysis was performed using two-
874 tailed unpaired Student's t-test (*** $p < 0.001$). **(D)** TEM micrograph shows HeLa HERPUD1-
875 WT-FLAG or HERPUD1-ΔUBL-FLAG (left and center images, respectively) at a lower
876 magnification. Crystalloid ER structure is visible as a honeycomb in HERPUD1-ΔUBL
877 (central image). An ER crystalloid structure from HERPUD1-ΔUBL-FLAG at a higher

878 magnification is shown (right image from dashed square in the center image, ER:
879 endoplasmic reticulum; M: mitochondria). Scale bar 500 nm.

880 **Figure 5. The stability of HERPUD1 by the deletion of its UBL domain does not trigger**
881 **endoplasmic reticulum stress. (A)** Splicing of *XBP1* was analyzed by RT-PCR. Total
882 RNAs were obtained from HeLa cells stably expressing HERPUD1-WT-FLAG or HERPUD1-
883 ΔUBL-FLAG, additionally, total RNA was obtained from HeLa WT cells untreated or treated
884 with 2 μM Thapsigargin (Tg) or 5 μg/mL Tunicamycin (Tun) for 4 h as a control of XBP1
885 splicing. Then, cDNA was synthesized and mRNA expression of XBP1 was analyzed using
886 specific primers. (*uXBP1*: unspliced form, *sXBP1*: spliced form). CYCLOPHILIN-A (CYC-A)
887 was used as an internal control. **(B)** HeLa cells stably expressing HERPUD1-WT-FLAG or
888 HERPUD1-ΔUBL-FLAG were treated with 2 μM Thapsigargin (Tg) for different timepoints (0
889 h, 2 h, 4 h and 6 h). Detergent-soluble protein extracts were analyzed by western blot with a
890 monoclonal antibody against XBP1. Monoclonal antibody against β-ACTIN was used as
891 loading control. Position of molecular mass markers is indicated on the left. **(C)** Densitometry
892 quantification of XBP1 protein levels from images as those shown in B. Bars represent the
893 mean ± standard deviation. Statistical analysis was performed using two-tailed unpaired
894 Student's t-test (n = 3 n.s not statistically significant, ** $p < 0.01$, *** $p < 0.001$).

895 **Figure 6. Expression of HERPUD1-ΔUBL increases lysosomal number and function.**
896 **(A)** HeLa cells stably expressing HERPUD1-WT-FLAG or HERPUD1-ΔUBL-FLAG grown in
897 glass coverslips were fixed, permeabilized and labeled with a mouse monoclonal antibody
898 against LAMP1 followed by incubation with Alexa-594-conjugated donkey anti-mouse IgG,
899 and DAPI for nuclei staining. Stained cells were examined by fluorescence microscopy.
900 Images were acquired using a TCS SP8 laser-scanning confocal microscope. Scale bar 10
901 μm. **(B)** Quantification of LAMP1 positive structures per cell. In the scatter plot each circle
902 and square represents the average of positive LAMP1 dots per cell from a frame of HeLa
903 HERPUD1-WT (n=559) or HERPUD1-ΔUBL (n=700) respectively. The quantified cells were
904 from 3 independent experiments. **(C and E)** HeLa cells stably expressing HERPUD1-WT-
905 FLAG or HERPUD1-ΔUBL-FLAG were grown in glass bottom culture dishes and labeled
906 with **(C)** LysoTracker™ Red DND-99 or **(E)** Magic Red®. For live cell imaging analysis,
907 culture medium was replaced with phenol red-free DMEM supplemented with HEPES (10
908 mM, pH 7.4) and images were acquired with TCS SP8 laser-scanning confocal microscope
909 at 37ºC. Scale bar 10 μm**. (D)** Quantification of LysoTracker™ dots per cell. Open circles
910 and open squares represent the average of fluorescence signals for each cell of HeLa
911 HERPUD1-WT-FLAG (n=139) or HERPUD1-ΔUBL-FLAG (n=138) respectively. **(F)**
912 Quantification of Magic Red® positive structures. In the scatter plot each circle and square
913 represents the average of positive dots for Magic Red per cell from a frame of HeLa
914 HERPUD1-WT-FLAG (n=1279) or HERPUD1-ΔUBL-FLAG (n=984) respectively. The
915 quantified cells were from 3 independent experiments. Statistical analysis was performed
916 using two-tailed unpaired Student's t-test (*** $p < 0.001$)

917 **Figure 7. Stabilization of HERPUD1 by S59D mutation alters the ER morphology and**
918 **decreases autophagy. (A)** HeLa cells stably expressing HERPUD1-WT-FLAG, HERPUD1-
919 S59A-FLAG or HERPUD1-S59D-FLAG were grown in glass coverslips, fixed, permeabilized,
920 and double-labeled with mouse monoclonal antibody against FLAG and with a rat
921 monoclonal antibody against GRP94 followed by incubation with Alexa-488-conjugated
922 donkey anti-rabbit IgG (green channel) and Alexa-594-conjugated donkey anti-rat IgG (red

923 channel). Images were acquired using a TCS SP8 laser-scanning confocal microscope. The
924 third image on each column is the merge of green and red channels; yellow indicates
925 colocalization of red and green channels. Scale bar: 10 μm. **(B)** Quantification of
926 fluorescence FLAG signal from indicated cells. **(C)** HeLa cells stably expressing HERPUD1-
927 WT-FLAG, HERPUD1-S59A-FLAG or HERPUD1-S59D-FLAG were treated or not with 10
928 μM of MG132 for 4 h. Detergent-soluble protein extracts were analyzed by western blot with
929 anti-HERPUD1 and anti-FLAG antibodies. β-ACTIN was used as a loading control. Position
930 of molecular mass markers is indicated on the left. **(D)** Densitometry quantification of
931 HERPUD1 western blot signal from images as those shown in C. Bars represent the mean ±
932 standard deviation. **(E)** HeLa cells stably expressing HERPUD1-WT-FLAG or HERPUD1-
933 S59D-FLAG untreated (lanes 1 and 3) or treated with 100 nM BafA1 for 4 h (lanes 2 and 4).
934 Detergent-soluble protein extracts were analyzed by western blot with a rabbit polyclonal
935 antibody to LC3B. Monoclonal antibody against β-ACTIN was used as a loading control.
936 Position of molecular mass markers is indicated on the left. **(F)** Densitometry quantification
937 of LC3-I and LC3-II protein levels from images as those shown in E. Relative levels are
938 expressed as the ratio of LC3-II to LC3-I from images as those shown in E. Bars represent
939 the mean ± standard deviation. Statistical analysis was performed using two-tailed unpaired
940 Student's t-test (n = 3 n.s. not statistically significant, *p < 0.05, ** p < 0.01, *** p < 0.001)
941
942 **Figure 8. Formation of lysosomal membrane contact sites with the extended ER**
943 **network in HERPUD1-ΔUBL and HERPUD1-S59D cells.** HeLa cells stably expressing
944 HERPUD1-WT-FLAG, HERPUD1-ΔUBL-FLAG or HERPUD1-S59D-FLAG were grown in
945 glass coverslips and then fixed, permeabilized and double-labeled with a rabbit monoclonal
946 antibody against CALNEXIN and a mouse monoclonal antibody against LAMP1 followed by
947 incubation with Alexa-488-conjugated donkey anti-rabbit IgG (green channel), Alexa-594-
948 conjugated donkey anti-mouse IgG (red channel) and DAPI for nuclei staining. All images
949 were acquired using a TCS SP8 laser-scanning confocal microscope in z-series. Upper
950 pannel correspond to inverted z-projection of maximum intensity of CALNEXIN images
951 showing the different ER patterns between cell lines. Middle pannel show 3D reconstructions
952 of CALNEXIN (green channel) and LAMP1 (red channel) images. Scale bar, 10 μm. Lower
953 pannel show a higher magnification of the 3D reconstructions. Scale bar, 1 μm (Note:
954 HERPUD1-WT-FLAG cells are smaller than HERPUD1-S59A-FLAG and HERPUD1-S59D-
955 FLAG).
956
957 **Figure 9. Stabilization of HERPUD1 by S59D mutation decreases cell death mediated**
958 **by CDDP. (A)** HeLa cells stably expressing HERPUD1-WT-FLAG or HERPUD1-S59D-
959 FLAG were treated with different concentrations of cisplatin (CDDP) and then a SRB assay
960 was performed. The absorbance values of each point were normalized to control cells
961 (without treatment) and transformed to a percentage. Experiments were performed at least
962 three times, and the results are expressed as mean ± standard deviation. Statistical analysis
963 was performed using two-tailed unpaired Student's t-test (n = 4 n.s. not statistically
964 significant and *p < 0.05) **(B)** HeLa cells stably expressing HERPUD1-WT-FLAG or
965 HERPUD1-S59D-FLAG were treated or not with CDDP 10 μM for 24 h. Afterwards, cells
966 were collected by trypsinization and stained with Annexin V-Pacific Blue and 7AAD. Scatter
967 plots representing the different quadrants are labeled as Q1 (necrotic cells), Q2 (viable
968 cells), Q3 (dead cells) and Q4 (apoptotic cells). The graph shows the percentage of cells
969 present in each quadrant.
970

971 **SUPPLEMENTARY FIGURE LEGENDS**
972
973 **Supplementary Figure 1.** Table summarizing all proteins identified as significantly differing
974 in abundance (Significance B <0.001) between normal and serum starved conditions for
975 either shLuc or shATG5 treated cells, or both. Number cells are color coded by response to
976 starvation; Blue = reduced abundance, red = increase, white = no change. Number Cells
977 with a black border met significance criteria. Blank number cells correspond to missing data
978 from one or both forward and reverse experiments.
979
980
981 **Supplementary Figure 2. The stabilization of HERPUD1 by its UBL deletion negatively**
982 **regulates autophagy under starvation**. **(A)** HeLa cells stably expressing HERPUD1-WT-
983 FLAG or HERPUD1-ΔUBL-FLAG untreated (lanes 1 and 2) or treated with EBSS for 4 h in
984 the absence or presence of 100 nM BafA1 (lanes 3 to 6). Detergent-soluble protein extracts
985 were analyzed by western blot with a rabbit polyclonal antibody against LC3. Monoclonal
986 antibody against β-ACTIN (clone BA3R) was used as a loading control. Position of molecular
987 mass markers is indicated on the left. **(B)** Densitometry quantification of LC3-I and LC3-II
988 protein levels from images as those shown in A. Relative levels are expressed as the ratio of
989 LC3-II to LC3-I. Bars represent the mean ± standard deviation. Statistical analysis was
990 performed using two-tailed unpaired Student's t-test (n = 3 * $p < 0.05$, ** $p < 0.01$).
991
992
993 **Supplementary Figure 3. HERPUD1-ΔUBL stabilization alters the ER morphology**
994 **without changing ER resident protein levels. (A)** HeLa cells stably expressing
995 HERPUD1-WT-FLAG or HERPUD1-ΔUBL-FLAG grown in glass coverslips were fixed,
996 permeabilized and incubated with an antibody against HERPUD1 followed by incubation with
997 Alexa-488-conjugated donkey anti-rabbit IgG. Stained cells were examined by confocal
998 microscopy. Scale bar 10 μm. **(B)** HeLa cells stably expressing HERPUD1-WT-FLAG or
999 HERPUD1-ΔUBL-FLAG were grown in glass bottom culture dishes and labeled with ER-
1000 Tracker™ Blue-White DPX. Stained cells were examined by fluorescence microscopy.
1001 Images were acquired using a TCS SP8 laser-scanning confocal microscope. Scale bar 10
1002 μm. **(C)** HeLa cells HERPUD1-WT-FLAG or HERPUD1-ΔUBL-FLAG. Detergent-soluble
1003 protein extracts were analyzed by western blot with a rabbit monoclonal antibody against
1004 CALNEXIN, rat monoclonal antibody against GRP94 and rabbit monoclonal antibody against
1005 HERPUD1. Monoclonal antibody against β-ACTIN (clone BA3R) was used as a loading
1006 control. Position of molecular mass markers is indicated on the left. **(D)** Densitometry
1007 quantification of CALNEXIN and GRP94 protein levels from images as those shown in C.
1008 Bars represent the mean ± standard deviation. Statistical analysis was performed using two-
1009 tailed unpaired Student's t-test (n = 3, n.s. not statistically significant).
1010
1011 **Supplementary Figure 4**. **The stability of HERPUD1 by the deletion of its UBL domain**
1012 **does not trigger endoplasmic reticulum stress.** HeLa WT cells untreated or treated with 2
1013 μM Thapsigargin (Tg) or 5 μg/mL Tunicamycin (Tun) for 4 h (lane 1 to 3) and untreated HeLa
1014 cells stably expressing HERPUD1-WT-FLAG or HERPUD1-ΔUBL-FLAG (lane 4 and 5) were
1015 lysed. Detergent-soluble protein extracts were analyzed by western blot with a rabbit
1016 polyclonal antibody against P-PERK/PERK, rabbit monoclonal antibody against ATF4 and
1017 rabbit monoclonal antibody against HERPUD1. Monoclonal antibody against β-ACTIN (clone

1018 BA3R) was used as a loading control. Position of molecular mass markers is indicated on
1019 the left.
1020
1021 **Supplementary Figure 5**. **Expression of HERPUD1-ΔUBL increases lysosomal**
1022 **organelle number. (A)** HeLa cells stably expressing HERPUD1-WT-FLAG or HERPUD1-
1023 ΔUBL-FLAG grown in glass coverslips were fixed, permeabilized, and double-labeled with
1024 mouse monoclonal antibody against LAMP1 and with a goat polyclonal antibody against
1025 CATHEPSIN-D (CAT-D) followed by incubation with Alexa-488-conjugated donkey anti-goat
1026 IgG (green channel), Alexa-594-conjugated donkey anti-mouse IgG (red channel) and DAPI
1027 for nuclei staining. Images were acquired using a TCS SP8 laser-scanning confocal
1028 microscope. The third image on each row is the merge of red and green channels; yellow
1029 indicates overlapping localization of the red and green channels. Scale bar, 10 μm. **(B)**
1030 Quantification of CATHEPSIN-D positive structures per cell. In the scatter plot open circles
1031 and open squares represent the average of fluorescence signal for each cell in a frame of
1032 HeLa HERPUD1-WT-FLAG (n=559) or HERPUD1-ΔUBL-FLAG (n=700) respectively.
1033 Quantified cells were from 3 independent experiments. Statistical analysis was performed
1034 using two-tailed unpaired Student's t-test (*** $p < 0.001$).
1035
1036 **Supplementary Figure 6. Predicted phosphorylation sites of the UBL domain in**
1037 **HERPUD1**. **(A)** The Ubiquitin-like Domain of HERPUD1 (PDB 1WGD, green color) and
1038 ubiquitin (PDB 2MSG, purple color) resolved structures were aligned by PyMOL molecular
1039 graphics system. **(B)** Predicted phosphorylated serines are shown in red in the resolved
1040 structure of the Ubiquitin-like Domain of HERPUD1 (PDB 1WGD, green color). Each arrow
1041 points to the specific residue shown in the figure.
1042
1043 **Supplementary Figure 7. Stabilization of HERPUD1 by S59D mutation decreases**
1044 **autophagosomes.** HeLa cells stably expressing HERPUD1-WT-FLAG or HERPUD1-S59D-
1045 FLAG grown in glass coverslips were treated or not with 100 nM BafA1 for 4 h. Cells were
1046 fixed, permeabilized and incubated with a polyclonal rabbit antibody against LC3 followed by
1047 incubation with Alexa-488-conjugated donkey anti-rabbit IgG. Stained cells were examined
1048 by confocal microscopy. Images were acquired using a TCS SP8 laser-scanning confocal
1049 microscope. Scale bar 10 μm.
1050
1051 **Supplementary Figure 8**. **Expression of HERPUD1-S59D increases nuclear and cell**
1052 **size. (A)** Cell size analysis of HeLa cells stably expressing HERPUD1-WT-FLAG,
1053 HERPUD1-ΔUBL-FLAG, HERPUD1-S59A-FLAG and HERPUD1-S59D-FLAG. Cells grown
1054 in glass coverslips were marked with Wheat Germ Agglutinin (WGA), fixed and stained with
1055 DAPI for nuclei visualization. Stained cells were examined by fluorescence microscopy. Cell
1056 area was measured by selection of cell contour. **(B)** Analysis of the nuclei size of HeLa
1057 HERPUD1-WT-FLAG, HERPUD1-ΔUBL-FLAG, HERPUD1-S59A-FLAG and HERPUD1-
1058 S59D-FLAG. Cells grown in glass coverslips were stained with Hoechst for nuclei
1059 visualization. Stained cells were examined by fluorescence microscopy. Nuclei area was
1060 measured by selection of nuclei contour.
1061
1062 **Supplementary Figure 9. Expression of HERPUD1-S59D increases lysosomal number**
1063 **and function. (A)** HeLa cells stably expressing HERPUD1-WT-FLAG, HERPUD1-S59A-
1064 FLAG or HERPUD1-S59D-FLAG grown in glass coverslips were fixed, permeabilized and
1065 labeled with a mouse monoclonal antibody against LAMP1 followed by incubation with

Alexa-594-conjugated donkey anti-mouse IgG and DAPI for nuclei staining. Stained cells were examined by fluorescence microscopy. Images were acquired using a TCS SP8 laser-scanning confocal microscope. Scale bar 10 μm. **(B)** Quantification of LAMP1 positive structures per cell. In the scatter plot each circle, triangle and rhombus represent the average of positive LAMP1 dots per cell from a frame of HeLa HERPUD1-WT-FLAG (n=559), HERPUD1-S59A-FLAG (n=557) and HERPUD1-S59D-FLAG (n=575) respectively. The quantified cells were from 3 independent experiments. **(C and E)** HeLa cells stably expressing HERPUD1-WT-FLAG, HERPUD1-S59A-FLAG or HERPUD1-S59D-FLAG were grown in glass bottom culture dishes and labeled with **(C)** LysoTracker™ Red DND-99 or **(E)** Magic Red®. For live cell imaging, cell culture medium was replaced with phenol red-free DMEM supplemented with HEPES (10 mM, pH 7.4), and images were acquired with TCS SP8 laser-scanning confocal microscope at 37ºC. Scale bar 10 μm**. (D)** Quantification of LysoTracker™ dots per cell. Open circles, triangles and rhombuses represent the average of fluorescence signals for each cell of HeLa HERPUD1-WT-FLAG (n=223), HERPUD1-S59A-FLAG (n=233) or HERPUD1-S59D-FLAG (n=124) respectively. **(F)** Quantification of Magic Red® positive structures. In the scatter plot each open circle, triangle and rhombus represent the average of positive dots for Magic Red per cell from a frame of HeLa HERPUD1-WT-FLAG (n=718), HERPUD1-S59A-FLAG (n=1183) or HERPUD1-S59D-FLAG (n=670) respectively. The quantified cells were from 3 independent experiments. Statistical analysis was performed using two-tailed unpaired Student's t-test (*** $p < 0.001$).

REFERENCES

Aguirre, Jacob D., Karen M. Dunkerley, Pascal Mercier, and Gary S. Shaw. 2017. "Structure of Phosphorylated UBL Domain and Insights into PINK1-Orchestrated Parkin Activation." *Proceedings of the National Academy of Sciences of the United States of America* 114(2): 298–303. https://pubmed.ncbi.nlm.nih.gov/28007983/ (March 30, 2021).

Anderson, R. G.W., L. Orci, and M. S. Brown. 1983. "Ultrastructural Analysis of Crystalloid Endoplasmic Reticulum in UT-1 Cells and Its Disappearance in Response to Cholesterol." *Journal of Cell Science*.

Antonioli, Manuela, Federica Albiero, Mauro Piacentini, and Gian Maria Fimia. 2016. "Temporal Regulation of Autophagy Response by the CULLIN 4-AMBRA1-CULLIN 5 Axis." *Molecular and Cellular Oncology* 3(5). https://pubmed.ncbi.nlm.nih.gov/27857967/ (March 30, 2021).

Asano, Shoh et al. 2015. "A Molecular Census of 26S Proteasomes in Intact Neurons." *Science* 347(6220): 439–42. https://pubmed.ncbi.nlm.nih.gov/25613890/ (March 30, 2021).

Ashrafizadeh, Milad, Zahra Ahmadi, Tahereh Farkhondeh, and Saeed Samarghandian. 2020. "Modulatory Effects of Statins on the Autophagy: A Therapeutic Perspective." *Journal of Cellular Physiology* 235(4): 3157–68. https://pubmed.ncbi.nlm.nih.gov/31578730/ (March 30, 2021).

Batista-Silva, Leonardo Ribeiro, Rychelle Clayde Affonso Medeiros, Flávio Alves Lara, and Milton Ozório Moraes. 2018. "Type I Interferons, Autophagy and Host Metabolism in Leprosy." *Frontiers in Immunology* 9(APR). https://pubmed.ncbi.nlm.nih.gov/29755459/ (March 30, 2021).

Benes, Petr, Vaclav Vetvicka, and Martin Fusek. 2008. "Cathepsin D-Many Functions of One Aspartic Protease." *Critical Reviews in Oncology/Hematology* 68(1): 12–28.

Bergmann, Timothy J. et al. 2018. "Chemical Stresses Fail to Mimic the Unfolded Protein Response Resulting from Luminal Load with Unfolded Polypeptides." *Journal of*

1117 *Biological Chemistry* 293(15): 5600–5612. https://pubmed.ncbi.nlm.nih.gov/29453283/
1118 (June 21, 2020).
1119 Bertolotti, Anne et al. 2000. "Dynamic Interaction of BiP and ER Stress Transducers in the
1120 Unfolded-Protein Response." *Nature Cell Biology* 2(6): 326–32.
1121 https://pubmed.ncbi.nlm.nih.gov/10854322/ (March 31, 2021).
1122 Blois, Joseph, Adam Smith, and Lee Josephson. 2011. "The Slow Cell Death Response
1123 When Screening Chemotherapeutic Agents." *Cancer Chemotherapy and Pharmacology*
1124 68(3): 795–803. https://pubmed.ncbi.nlm.nih.gov/21193989/ (March 30, 2021).
1125 Boonacker, Emil et al. 2003. "Rapid Assay to Detect Possible Natural Substrates of
1126 Proteases in Living Cells." *BioTechniques* 35(4): 766–74.
1127 https://pubmed.ncbi.nlm.nih.gov/14579742/ (March 31, 2021).
1128 Borgese, Nica, Maura Francolini, and Erik Snapp. 2006. "Endoplasmic Reticulum
1129 Architecture : Structures in Flux." *Current Opinion in Cell Biology* 18(4): 358–64.
1130 https://pubmed.ncbi.nlm.nih.gov/16806883/ (March 30, 2021).
1131 Bustamante, Hianara A. et al. 2018. "Interplay between the Autophagy-Lysosomal Pathway
1132 and the Ubiquitin-Proteasome System: A Target for Therapeutic Development in
1133 Alzheimer's Disease." *Frontiers in Cellular Neuroscience* 12.
1134 https://pubmed.ncbi.nlm.nih.gov/29867359/ (March 30, 2021).
1135 Bustamante, Hianara A et al. 2020. "The Proteasomal Deubiquitinating Enzyme PSMD14
1136 Regulates Macroautophagy by Controlling Golgi-to-ER Retrograde Transport." *Cells*
1137 9(3): 777. https://pubmed.ncbi.nlm.nih.gov/32210007/ (June 23, 2020).
1138 Caldieri, Giusi et al. 2017. "Reticulon 3-Dependent ER-PM Contact Sites Control EGFR
1139 Nonclathrin Endocytosis." *Science* 356(6338): 617–24.
1140 https://pubmed.ncbi.nlm.nih.gov/28495747/ (March 30, 2021).
1141 Camuzard, Olivier, Sabine Santucci-Darmanin, Georges F. Carle, and Valérie Pierrefite-
1142 Carle. 2020. "Autophagy in the Crosstalk between Tumor and Microenvironment."
1143 *Cancer Letters* 490: 143–53. https://pubmed.ncbi.nlm.nih.gov/32634449/ (March 30,
1144 2021).
1145 Cavieres, Viviana A. et al. 2020. "Human Golgi Phosphoprotein 3 Is an Effector of RAB1A
1146 and RAB1B." *PLoS ONE* 15(8 August). https://pubmed.ncbi.nlm.nih.gov/32790781/
1147 (March 30, 2021).
1148 Chin, D. J. et al. 1982. "Appearance of Crystalloid Endoplasmic Reticulum in Compactin-
1149 Resistant Chinese Hamster Cells with a 500-Fold Increase in 3-Hydroxy-3-
1150 Methylglutaryl-Coenzyme A Reductase." *Proceedings of the National Academy of*
1151 *Sciences of the United States of America* 79(4 I): 1185–89.
1152 https://pubmed.ncbi.nlm.nih.gov/6951166/ (March 30, 2021).
1153 Chou, Kai Ming, A. Paul Krapcho, and Miles P. Hacker. 2001. "Impact of the Basic Amine on
1154 the Biological Activity and Intracellular Distribution of an Aza-Anthrapyrazole: BBR
1155 3422." *Biochemical Pharmacology* 62(10): 1337–43.
1156 https://pubmed.ncbi.nlm.nih.gov/11709193/ (March 30, 2021).
1157 Collins, Galen A., and Alfred L. Goldberg. 2020. "Proteins Containing Ubiquitin-like (Ubl)
1158 Domains Not Only Bind to 26S Proteasomes but Also Induce Their Activation."
1159 *Proceedings of the National Academy of Sciences of the United States of America*
1160 117(9): 4664–74. https://pubmed.ncbi.nlm.nih.gov/32071216/ (March 30, 2021).
1161 Dasari, Shaloam, and Paul Bernard Tchounwou. 2014. "Cisplatin in Cancer Therapy:
1162 Molecular Mechanisms of Action." *European Journal of Pharmacology* 740: 364–78.
1163 https://pubmed.ncbi.nlm.nih.gov/25058905/ (March 30, 2021).
1164 Demishtein, Alik et al. 2017. "SQSTM1/P62-Mediated Autophagy Compensates for Loss of
1165 Proteasome Polyubiquitin Recruiting Capacity." *Autophagy* 13(10): 1697–1708.
1166 https://pubmed.ncbi.nlm.nih.gov/28792301/ (March 30, 2021).
1167 De Duve, Christian et al. 1974. "Lysosomotropic Agents." *Biochemical Pharmacology* 23(18).
1168 https://pubmed.ncbi.nlm.nih.gov/4606365/ (March 30, 2021).
1169 Feldman, Dorothy, Richard L. Swarm, and Janet Becker. 1981. "Ultrastructural Study of Rat
1170 Liver and Liver Neoplasms after Long-Term Treatment with Phenobarbital." *Cancer*
1171 *Research*.

1172 Fregno, Ilaria et al. 2018. " ER -to-lysosome-associated Degradation of Proteasome-
1173 resistant ATZ Polymers Occurs via Receptor-mediated Vesicular Transport ." *The*
1174 *EMBO Journal* 37(17). https://pubmed.ncbi.nlm.nih.gov/30076131/ (March 30, 2021).
1175 Fregno, Ilaria, and Maurizio Molinari. 2019. "Proteasomal and Lysosomal Clearance of
1176 Faulty Secretory Proteins: ER-Associated Degradation (ERAD) and ER-to-Lysosome-
1177 Associated Degradation (ERLAD) Pathways." *Critical Reviews in Biochemistry and*
1178 *Molecular Biology* 54(2): 153–63. https://pubmed.ncbi.nlm.nih.gov/31084437/ (March
1179 30, 2021).
1180 Friedman, Jonathan R. et al. 2013. "Endoplasmic Reticulum-Endosome Contact Increases
1181 as Endosomes Traffic and Mature." *Molecular Biology of the Cell* 24(7): 1030–40.
1182 https://pubmed.ncbi.nlm.nih.gov/23389631/ (March 30, 2021).
1183 Golebiowski, Filip et al. 2009. "System-Wide Changes to Sumo Modifications in Response to
1184 Heat Shock." *Science Signaling* 2(72). https://pubmed.ncbi.nlm.nih.gov/19471022/
1185 (March 30, 2021).
1186 González, Alexis E. et al. 2017. "Autophagosomes Cooperate in the Degradation of
1187 Intracellular C-Terminal Fragments of the Amyloid Precursor Protein via the
1188 MVB/Lysosomal Pathway." *FASEB Journal* 31(6): 2446–59.
1189 https://pubmed.ncbi.nlm.nih.gov/28254759/ (June 23, 2020).
1190 Griffiths, Gareth et al. 1988. "The Mannose 6-Phosphate Receptor and the Biogenesis of
1191 Lysosomes." *Cell* 52(3): 329–41. https://pubmed.ncbi.nlm.nih.gov/2964276/ (March 30,
1192 2021).
1193 Grumati, Paolo, Ivan Dikic, and Alexandra Stolz. 2018. "ER-Phagy at a Glance." *Journal of*
1194 *Cell Science* 131(17). https://pubmed.ncbi.nlm.nih.gov/30177506/ (March 30, 2021).
1195 Guarascio, Rosellina et al. 2020. "Negative Regulator of Ubiquitin-Like Protein 1 Modulates
1196 the Autophagy-Lysosomal Pathway via P62 to Facilitate the Extracellular Release of
1197 Tau Following Proteasome Impairment." *Human Molecular Genetics* 29(1): 80–96.
1198 https://pubmed.ncbi.nlm.nih.gov/31691796/ (March 30, 2021).
1199 Harding, Heather P., Yuhong Zhang, et al. 2000. "Perk Is Essential for Translational
1200 Regulation and Cell Survival during the Unfolded Protein Response." *Molecular Cell*
1201 5(5): 897–904. https://pubmed.ncbi.nlm.nih.gov/10882126/ (March 30, 2021).
1202 Harding, Heather P., Isabel Novoa, et al. 2000. "Regulated Translation Initiation Controls
1203 Stress-Induced Gene Expression in Mammalian Cells." *Molecular Cell* 6(5): 1099–1108.
1204 https://pubmed.ncbi.nlm.nih.gov/11106749/ (March 30, 2021).
1205 Hartmann-Petersen, R., and C. Gordon. 2004. "Ubiquitin-Proteasome System." *Cellular and*
1206 *Molecular Life Sciences* 61(13). https://pubmed.ncbi.nlm.nih.gov/15224183/ (March 30,
1207 2021).
1208 Hartmann-Petersen, Rasmus, and Colin Gordon. 2004. "Integral UBL Domain Proteins: A
1209 Family of Proteasome Interacting Proteins." *Seminars in Cell and Developmental*
1210 *Biology* 15(2): 247–59. https://pubmed.ncbi.nlm.nih.gov/15209385/ (March 30, 2021).
1211 Heifetz, Aaron, Roy W. Keenan, and Alan D. Elbein. 1979. "Mechanism of Action of
1212 Tunicamycin on the UDP-GlcNAc:Dolichyl-Phosphate GlcNAc-1 -Phosphate
1213 Transferase." *Biochemistry* 18(11): 2186–92.
1214 https://pubs.acs.org/doi/abs/10.1021/bi00578a008 (April 27, 2021).
1215 Henne, William Mike. 2017. "Discovery and Roles of ER-Endolysosomal Contact Sites in
1216 Disease." *Advances in experimental medicine and biology* 997: 135–47.
1217 https://pubmed.ncbi.nlm.nih.gov/28815527/ (March 30, 2021).
1218 Huber, Michael D., and Larry Gerace. 2007. "The Size-Wise Nucleus: Nuclear Volume
1219 Control in Eukaryotes." *Journal of Cell Biology* 179(4): 583–84.
1220 https://pubmed.ncbi.nlm.nih.gov/17998404/ (March 30, 2021).
1221 Jackson, Matthew P., and Eric W. Hewitt. 2016. "Cellular Proteostasis: Degradation of
1222 Misfolded Proteins by Lysosomes." *Essays in Biochemistry* 60(2): 173–80.
1223 https://pubmed.ncbi.nlm.nih.gov/27744333/ (March 30, 2021).
1224 Jia, Rui, and Juan S. Bonifacino. 2019. "Negative Regulation of Autophagy by Uba6-Birc6–
1225 Mediated Ubiquitination of Lc3." *eLife* 8. https://pubmed.ncbi.nlm.nih.gov/31692446/
1226 (March 30, 2021).

1227 Jin, Seok Min, and Richard J. Youle. 2012. “PINK1-and Parkin-Mediated Mitophagy at a
1228 Glance.” *Journal of Cell Science* 125(4): 795–99.
1229 https://pubmed.ncbi.nlm.nih.gov/22448035/ (March 30, 2021).
1230 Jung, Hye Seung et al. 2008. “Loss of Autophagy Diminishes Pancreatic β Cell Mass and
1231 Function with Resultant Hyperglycemia.” *Cell Metabolism* 8(4): 318–24.
1232 https://pubmed.ncbi.nlm.nih.gov/18840362/ (April 26, 2021).
1233 Khaminets, Aliaksandr et al. 2015. “Regulation of Endoplasmic Reticulum Turnover by
1234 Selective Autophagy.” *Nature* 522(7556): 354–58.
1235 https://pubmed.ncbi.nlm.nih.gov/26040720/ (March 30, 2021).
1236 Khaminets, Aliaksandr, Christian Behl, and Ivan Dikic. 2016. “Ubiquitin-Dependent And
1237 Independent Signals In Selective Autophagy.” *Trends in Cell Biology* 26(1): 6–16.
1238 https://pubmed.ncbi.nlm.nih.gov/26437584/ (March 30, 2021).
1239 Kim, Eunkyoung et al. 2018. “Dual Function of USP14 Deubiquitinase in Cellular
1240 Proteasomal Activity and Autophagic Flux.” *Cell Reports* 24(3): 732–43.
1241 https://pubmed.ncbi.nlm.nih.gov/30021169/ (March 30, 2021).
1242 Kim, Hyoung Tae, and Alfred L. Goldberg. 2018. “UBL Domain of Usp14 and Other Proteins
1243 Stimulates Proteasome Activities and Protein Degradation in Cells.” *Proceedings of the*
1244 *National Academy of Sciences of the United States of America* 115(50): E11642–50.
1245 https://pubmed.ncbi.nlm.nih.gov/30487212/ (March 30, 2021).
1246 Kim, Tae Yeon, Eunmin Kim, Sungjoo Kim Yoon, and Jong Bok Yoon. 2008. “Herp
1247 Enhances ER-Associated Protein Degradation by Recruiting Ubiquilins.” *Biochemical*
1248 *and Biophysical Research Communications* 369(2): 741–46.
1249 https://pubmed.ncbi.nlm.nih.gov/18307982/ (March 30, 2021).
1250 Kokame, K., K. L. Agarwal, H. Kato, and T. Miyata. 2000. “Herp, a New Ubiquitin-like
1251 Membrane Protein Induced by Endoplasmic Reticulum Stress.” *Journal of Biological*
1252 *Chemistry* 275(42): 32846–53. https://pubmed.ncbi.nlm.nih.gov/10922362/ (June 21,
1253 2020).
1254 Kokame, Koichi, Hisao Kato, and Toshiyuki Miyata. 2001. “Identification of ERSE-II, a New
1255 Cis-Acting Element Responsible for the ATF6-Dependent Mammalian Unfolded Protein
1256 Response.” *Journal of Biological Chemistry* 276(12): 9199–9205.
1257 https://pubmed.ncbi.nlm.nih.gov/11112790/ (March 30, 2021).
1258 Kondapalli, Chandana et al. 2012. “PINK1 Is Activated by Mitochondrial Membrane Potential
1259 Depolarization and Stimulates Parkin E3 Ligase Activity by Phosphorylating Serine 65.”
1260 *Open Biology* 2(MAY). https://pubmed.ncbi.nlm.nih.gov/22724072/ (March 30, 2021).
1261 Korolchuk, Viktor I., Fiona M. Menzies, and David C. Rubinsztein. 2010. “Mechanisms of
1262 Cross-Talk between the Ubiquitin-Proteasome and Autophagy-Lysosome Systems.”
1263 *FEBS Letters* 584(7): 1393–98. https://pubmed.ncbi.nlm.nih.gov/20040365/ (March 30,
1264 2021).
1265 Koyano, Fumika et al. 2014. “Ubiquitin Is Phosphorylated by PINK1 to Activate Parkin.”
1266 *Nature* 510(7503): 162–66. https://pubmed.ncbi.nlm.nih.gov/24784582/ (June 24,
1267 2020).
1268 Van Der Laan, Sander W. et al. 2018. “From Lipid Locus to Drug Target through Human
1269 Genomics.” *Cardiovascular Research* 114(9): 1258–70.
1270 https://pubmed.ncbi.nlm.nih.gov/29800275/ (March 30, 2021).
1271 Lee, Crystal A., and Craig Blackstone. 2020. “ER Morphology and Endo-Lysosomal
1272 Crosstalk: Functions and Disease Implications.” *Biochimica et Biophysica Acta -*
1273 *Molecular and Cell Biology of Lipids* 1865(1).
1274 https://pubmed.ncbi.nlm.nih.gov/31678515/ (March 30, 2021).
1275 Lee, Do Hee. 1998. “Proteasome Inhibitors: Valuable New Tools for Cell Biologists.” *Trends*
1276 *in Cell Biology* 8(10): 397–403. https://pubmed.ncbi.nlm.nih.gov/9789328/ (March 30,
1277 2021).
1278 Leitman, Julia et al. 2014. “Herp Coordinates Compartmentalization and Recruitment of
1279 HRD1 and Misfolded Proteins for ERAD.” *Molecular Biology of the Cell* 25(7): 1050–60.
1280 https://pubmed.ncbi.nlm.nih.gov/24478453/ (June 23, 2020).
1281 Liao, Yangjie et al. 2019. “Excessive ER-Phagy Mediated by the Autophagy Receptor

FAM134B Results in ER Stress, the Unfolded Protein Response, and Cell Death in HeLa Cells." *Journal of Biological Chemistry* 294(52): 20009–23. https://pubmed.ncbi.nlm.nih.gov/31748416/ (March 30, 2021).

Marzec, Michal, Davide Eletto, and Yair Argon. 2012. "GRP94: An HSP90-like Protein Specialized for Protein Folding and Quality Control in the Endoplasmic Reticulum." *Biochimica et Biophysica Acta - Molecular Cell Research* 1823(3): 774–87. https://pubmed.ncbi.nlm.nih.gov/22079671/ (March 31, 2021).

Miettinen, Teemu P., and Mikael Björklund. 2015. "Mevalonate Pathway Regulates Cell Size Homeostasis and Proteostasis through Autophagy." *Cell Reports* 13(11): 2610–20. https://pubmed.ncbi.nlm.nih.gov/26686643/ (March 30, 2021).

Miura, Hikari et al. 2010. "Deletion of Herp Facilitates Degradation of Cytosolic Proteins." *Genes to Cells* 15(8): 843–53. https://pubmed.ncbi.nlm.nih.gov/20604806/ (March 30, 2021).

Mizushima, Noboru, Beth Levine, Ana Maria Cuervo, and Daniel J. Klionsky. 2008. "Autophagy Fights Disease through Cellular Self-Digestion." *Nature* 451(7182): 1069–75. https://pubmed.ncbi.nlm.nih.gov/18305538/ (March 30, 2021).

Mizushima, Noboru, Tamotsu Yoshimori, and Yoshinori Ohsumi. 2011. "The Role of Atg Proteins in Autophagosome Formation." *Annual Review of Cell and Developmental Biology* 27: 107–32. https://pubmed.ncbi.nlm.nih.gov/21801009/ (March 30, 2021).

Mollazadeh, Hamid et al. 2018. "The Effect of Statin Therapy on Endoplasmic Reticulum Stress." *Pharmacological Research* 137: 150–58. https://pubmed.ncbi.nlm.nih.gov/30312664/ (March 30, 2021).

Moreau, Kevin, Shouqing Luo, and David C. Rubinsztein. 2010. "Cytoprotective Roles for Autophagy." *Current Opinion in Cell Biology* 22(2): 206–11. https://pubmed.ncbi.nlm.nih.gov/20045304/ (March 30, 2021).

Murrow, Lyndsay, and Jayanta Debnath. 2013. "Autophagy as a Stress-Response and Quality-Control Mechanism: Implications for Cell Injury and Human Disease." *Annual Review of Pathology: Mechanisms of Disease* 8: 105–37. https://pubmed.ncbi.nlm.nih.gov/23072311/ (March 30, 2021).

Neefjes, Jacques, Marlieke M.L. Jongsma, and Ilana Berlin. 2017. "Stop or Go? Endosome Positioning in the Establishment of Compartment Architecture, Dynamics, and Function." *Trends in Cell Biology* 27(8): 580–94. https://pubmed.ncbi.nlm.nih.gov/28363667/ (March 30, 2021).

Ou, W. J. et al. 1995. "Conformational Changes Induced in the Endoplasmic Reticulum Luminal Domain of Calnexin by Mg-ATP and Ca2+." *Journal of Biological Chemistry* 270(30): 18051–59. https://pubmed.ncbi.nlm.nih.gov/7629114/ (March 30, 2021).

Quiroga, Clara et al. 2013. "Herp Depletion Protects from Protein Aggregation by Up-Regulating Autophagy." *Biochimica et Biophysica Acta - Molecular Cell Research* 1833(12): 3295–3305. https://pubmed.ncbi.nlm.nih.gov/24120520/ (March 30, 2021).

Rothenberg, Cara et al. 2010. "Ubiquilin Functions in Autophagy and Is Degraded by Chaperone-Mediated Autophagy." *Human Molecular Genetics* 19(16): 3219–32. https://pubmed.ncbi.nlm.nih.gov/20529957/ (March 30, 2021).

Sai, Xiaorei et al. 2003. "The Ubiquitin-like Domain of Herp Is Involved in Herp Degradation, but Not Necessary for Its Enhancement of Amyloid β-Protein Generation." *FEBS Letters* 553(1–2): 151–56. https://pubmed.ncbi.nlm.nih.gov/14550564/ (March 30, 2021).

Sauvé, Véronique et al. 2018. "Mechanism of Parkin Activation by Phosphorylation." *Nature Structural and Molecular Biology* 25(7): 623–30. https://pubmed.ncbi.nlm.nih.gov/29967542/ (March 30, 2021).

Schindelin, Johannes et al. 2012. "Fiji: An Open-Source Platform for Biological-Image Analysis." *Nature Methods* 9(7): 676–82. https://pubmed.ncbi.nlm.nih.gov/22743772/ (March 30, 2021).

Schuck, Sebastian et al. 2009. "Membrane Expansion Alleviates Endoplasmic Reticulum Stress Independently of the Unfolded Protein Response." *Journal of Cell Biology* 187(4): 525–36. https://pubmed.ncbi.nlm.nih.gov/19948500/ (March 30, 2021).

Schulz, Jasmin et al. 2017. "Conserved Cytoplasmic Domains Promote Hrd1 Ubiquitin

Ligase Complex Formation for ER-Associated Degradation (ERAD)." *Journal of Cell Science* 130(19): 3322–35. https://pubmed.ncbi.nlm.nih.gov/28827405/ (March 30, 2021).

Schulze, Andrea et al. 2005. "The Ubiquitin-Domain Protein HERP Forms a Complex with Components of the Endoplasmic Reticulum Associated Degradation Pathway." *Journal of Molecular Biology* 354(5): 1021–27. https://pubmed.ncbi.nlm.nih.gov/16289116/ (March 30, 2021).

Sebti, Salwa et al. 2014. "BAT3 Modulates P300-Dependent Acetylation of P53 and Autophagy-Related Protein 7 (ATG7) during Autophagy." *Proceedings of the National Academy of Sciences of the United States of America* 111(11): 4115–20. https://pubmed.ncbi.nlm.nih.gov/24591579/ (March 30, 2021).

Şentürk, Mümine et al. 2019. "Ubiquilins Regulate Autophagic Flux through MTOR Signalling and Lysosomal Acidification." *Nature Cell Biology* 21(3): 384–96. https://pubmed.ncbi.nlm.nih.gov/30804504/ (March 30, 2021).

Shi, Xiaojuan et al. 2020. "Silencing UHRF1 Enhances Cell Autophagy to Prevent Articular Chondrocytes from Apoptosis in Osteoarthritis through PI3K/AKT/MTOR Signaling Pathway." *Biochemical and Biophysical Research Communications* 529(4): 1018–24. https://pubmed.ncbi.nlm.nih.gov/32819559/ (March 30, 2021).

Swaney, Danielle L, Ricard A Rodríguez-Mias, and Judit Villén. 2015. "Phosphorylation of Ubiquitin at Ser65 Affects Its Polymerization, Targets, and Proteome-wide Turnover." *EMBO reports* 16(9): 1131–44. https://pubmed.ncbi.nlm.nih.gov/26142280/ (June 24, 2020).

Tanida, Isei, Takashi Ueno, and Eiki Kominami. 2008. "LC3 and Autophagy." *Methods in Molecular Biology* 445: 77–88. https://pubmed.ncbi.nlm.nih.gov/18425443/ (March 30, 2021).

Tapia, Diego et al. 2019. "KDEL Receptor Regulates Secretion by Lysosome Relocation- and Autophagy-Dependent Modulation of Lipid-Droplet Turnover." *Nature Communications* 10(1). https://pubmed.ncbi.nlm.nih.gov/30760704/ (March 30, 2021).

Thastrup, O et al. 1990. "Thapsigargin, a Tumor Promoter, Discharges Intracellular Ca2+ Stores by Specific Inhibition of the Endoplasmic Reticulum Ca2(+)-ATPase." *Proceedings of the National Academy of Sciences* 87(7).

Thayer, Julia A. et al. 2020. "The PARK10 Gene USP24 Is a Negative Regulator of Autophagy and ULK1 Protein Stability." *Autophagy* 16(1): 140–53. https://pubmed.ncbi.nlm.nih.gov/30957634/ (March 30, 2021).

Toulmay, Alexandre, and William A. Prinz. 2011. "Lipid Transfer and Signaling at Organelle Contact Sites: The Tip of the Iceberg." *Current Opinion in Cell Biology* 23(4): 458–63. https://pubmed.ncbi.nlm.nih.gov/21555211/ (March 30, 2021).

Tsubuki, Satoshi et al. 1996. "Differential Inhibition of Calpain and Proteasome Activities by Peptidyl Aldehydes of Di-Leucine and Tri-Leucine." *Journal of Biochemistry* 119(3): 572–76. https://pubmed.ncbi.nlm.nih.gov/8830056/ (March 30, 2021).

Vabulas, Ramunas M., and F. Ulrich Hartl. 2005. "Cell Biology: Protein Synthesis upon Acute Nutrient Restriction Relies on Proteasome Function." *Science* 310(5756): 1960–63. https://pubmed.ncbi.nlm.nih.gov/16373576/ (March 30, 2021).

Valm, Alex M. et al. 2017. "Applying Systems-Level Spectral Imaging and Analysis to Reveal the Organelle Interactome." *Nature* 546(7656): 162–67. https://pubmed.ncbi.nlm.nih.gov/28538724/ (March 30, 2021).

VerPlank, Jordan J.S., Sudarsanareddy Lokireddy, Jinghui Zhao, and Alfred L. Goldberg. 2019. "26S Proteasomes Are Rapidly Activated by Diverse Hormones and Physiological States That Raise CAMP and Cause Rpn6 Phosphorylation." *Proceedings of the National Academy of Sciences of the United States of America* 116(10): 4228–37. https://pubmed.ncbi.nlm.nih.gov/30782827/ (March 30, 2021).

Walczak, Marta, and Sascha Martens. 2013. "Dissecting the Role of the Atg12-Atg5-Atg16 Complex during Autophagosome Formation." *Autophagy* 9(3): 424–25. https://pubmed.ncbi.nlm.nih.gov/23321721/ (March 30, 2021).

Wauer, Tobias et al. 2015. "Ubiquitin Ser65 Phosphorylation Affects Ubiquitin Structure,

1392 Chain Assembly and Hydrolysis." *The EMBO Journal* 34(3): 307–25.
1393 https://pubmed.ncbi.nlm.nih.gov/25527291/ (March 30, 2021).
1394 Wiest, D. L. et al. 1990. "Membrane Biogenesis during B Cell Differentiation: Most
1395 Endoplasmic Reticulum Proteins Are Expressed Coordinately." *Journal of Cell Biology*
1396 110(5): 1501–11. https://pubmed.ncbi.nlm.nih.gov/2335560/ (March 30, 2021).
1397 Wu, Yuping et al. 2018. "Alleviation of Endoplasmic Reticulum Stress Protects against
1398 Cisplatin-Induced Ovarian Damage." *Reproductive Biology and Endocrinology* 16(1).
1399 https://pubmed.ncbi.nlm.nih.gov/30176887/ (March 30, 2021).
1400 Xu, Fang et al. 2021. "COPII Mitigates ER Stress by Promoting Formation of ER Whorls."
1401 *Cell Research* 31(2): 141–56. https://pubmed.ncbi.nlm.nih.gov/32989223/ (March 30,
1402 2021).
1403 Xu, Haoxing, and Dejian Ren. 2015. "Lysosomal Physiology." *Annual Review of Physiology*
1404 77: 57–80. https://pubmed.ncbi.nlm.nih.gov/25668017/ (March 30, 2021).
1405 Yan, Long et al. 2014. "Ube2g2-Gp78-Mediated HERP Polyubiquitylation Is Involved in ER
1406 Stress Recovery." Journal of Cell Science 127(7): 1417–27.
1407 https://pubmed.ncbi.nlm.nih.gov/24496447/ (June 21, 2020).
1408 Yang, Ying, and Daniel J. Klionsky. 2020. "A Novel Role of UBQLNs (Ubiquilins) in
1409 Regulating Autophagy, MTOR Signaling and v-ATPase Function." *Autophagy* 16(1): 1–
1410 2. https://pubmed.ncbi.nlm.nih.gov/31516068/ (March 30, 2021).
1411 Yin, Yili et al. 2012. "SUMO-Targeted Ubiquitin E3 Ligase RNF4 Is Required for the
1412 Response of Human Cells to DNA Damage." *Genes and Development* 26(11): 1196–
1413 1208. https://pubmed.ncbi.nlm.nih.gov/22661230/ (March 30, 2021).
1414 Yoshida, Hiderou et al. 2001. "XBP1 MRNA Is Induced by ATF6 and Spliced by IRE1 in
1415 Response to ER Stress to Produce a Highly Active Transcription Factor." *Cell* 107(7):
1416 881–91. https://pubmed.ncbi.nlm.nih.gov/11779464/ (March 30, 2021).
1417 Yu, Houqing, and Andreas Matouschek. 2017. "Recognition of Client Proteins by the
1418 Proteasome." *Annual Review of Biophysics* 46: 149–73.
1419 https://pubmed.ncbi.nlm.nih.gov/28301771/ (March 30, 2021).
1420 Zhang, Tao et al. 2018. "HMG-CoA Reductase Inhibitors Relieve Endoplasmic Reticulum
1421 Stress by Autophagy Inhibition in Rats with Permanent Brain Ischemia." *Frontiers in*
1422 *Neuroscience* 12(JUN). https://pubmed.ncbi.nlm.nih.gov/29970982/ (March 30, 2021).
1423 Zhang, Youzhi et al. 2020. "Simvastatin Improves Lysosome Function via Enhancing
1424 Lysosome Biogenesis in Endothelial Cells." *Frontiers in Bioscience - Landmark*.
1425 Zhu, K., K. Dunner, and D. J. McConkey. 2010. "Proteasome Inhibitors Activate Autophagy
1426 as a Cytoprotective Response in Human Prostate Cancer Cells." *Oncogene* 29(3): 451–
1427 62. https://pubmed.ncbi.nlm.nih.gov/19881538/ (March 30, 2021).
1428

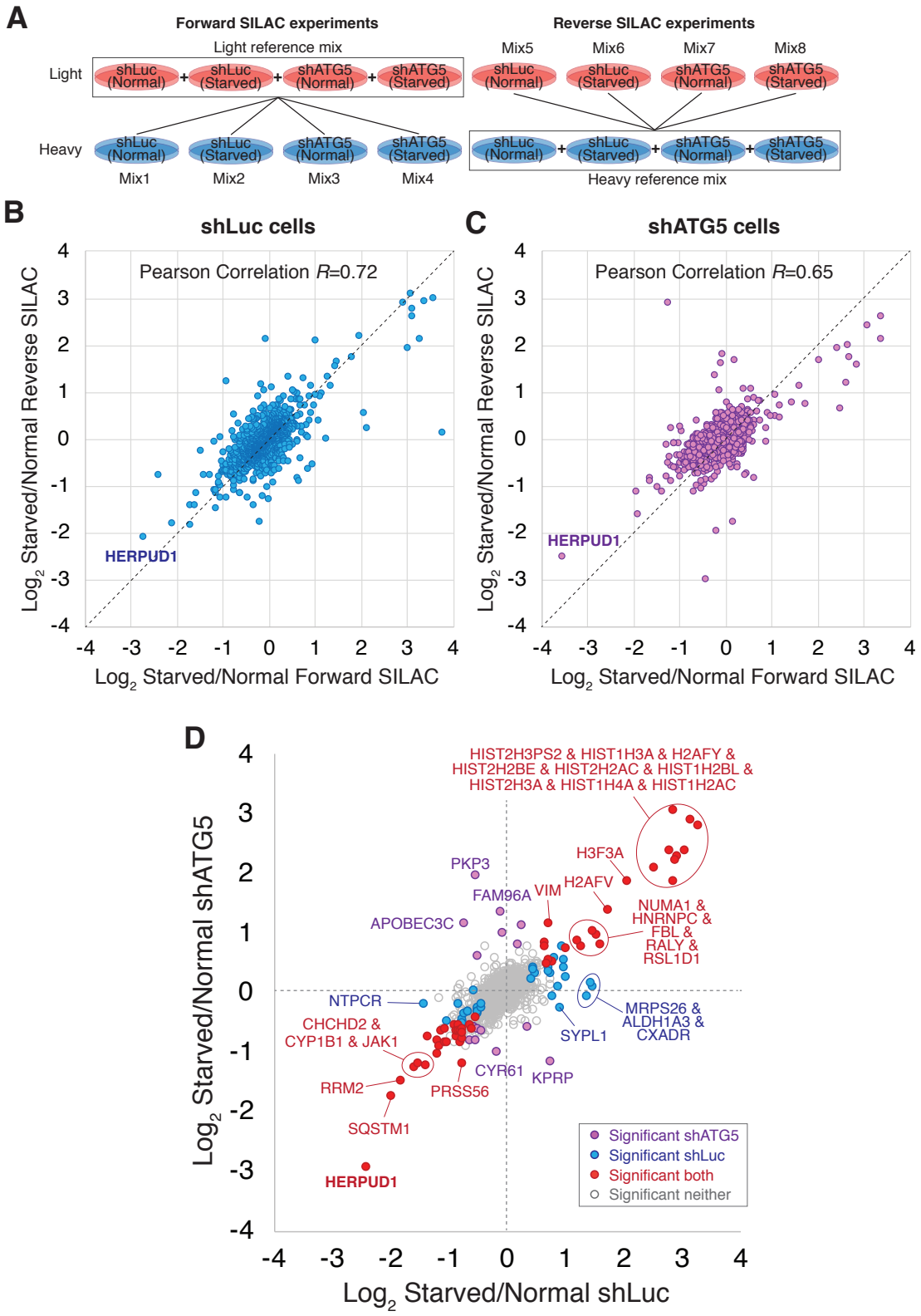
A
Forward SILAC experiments
Light reference mix
Light
shLuc (Normal)
shLuc (Starved)
shATG5 (Normal)
shATG5 (Starved)
Heavy
Mix1
Mix2
Mix3
Mix4
Reverse SILAC experiments
Mix5
Mix6
Mix7
Mix8
Heavy reference mix
B
shLuc cells
Pearson Correlation R=0.72
HERPUD1
Log2 Starved/Normal Reverse SILAC
Log2 Starved/Normal Forward SILAC
C
shATG5 cells
Pearson Correlation R=0.65
HERPUD1
Log2 Starved/Normal Reverse SILAC
Log2 Starved/Normal Forward SILAC
D
HIST2H3PS2 & HIST1H3A & H2AFY & HIST2H2BE & HIST2H2AC & HIST1H2BL & HIST2H3A & HIST1H4A & HIST1H2AC
H3F3A
H2AFV
PKP3
FAM96A
VIM
APOBEC3C
NUMA1 & HNRNPC & FBL & RALY & RSL1D1
NTPCR
MRPS26 & ALDH1A3 & CXADR
SYPL1
CHCHD2 & CYP1B1 & JAK1
CYR61
KPRP
RRM2
PRSS56
SQSTM1
HERPUD1
Significant shATG5
Significant shLuc
Significant both
Significant neither
Log2 Starved/Normal shATG5
Log2 Starved/Normal shLuc

Figure 1

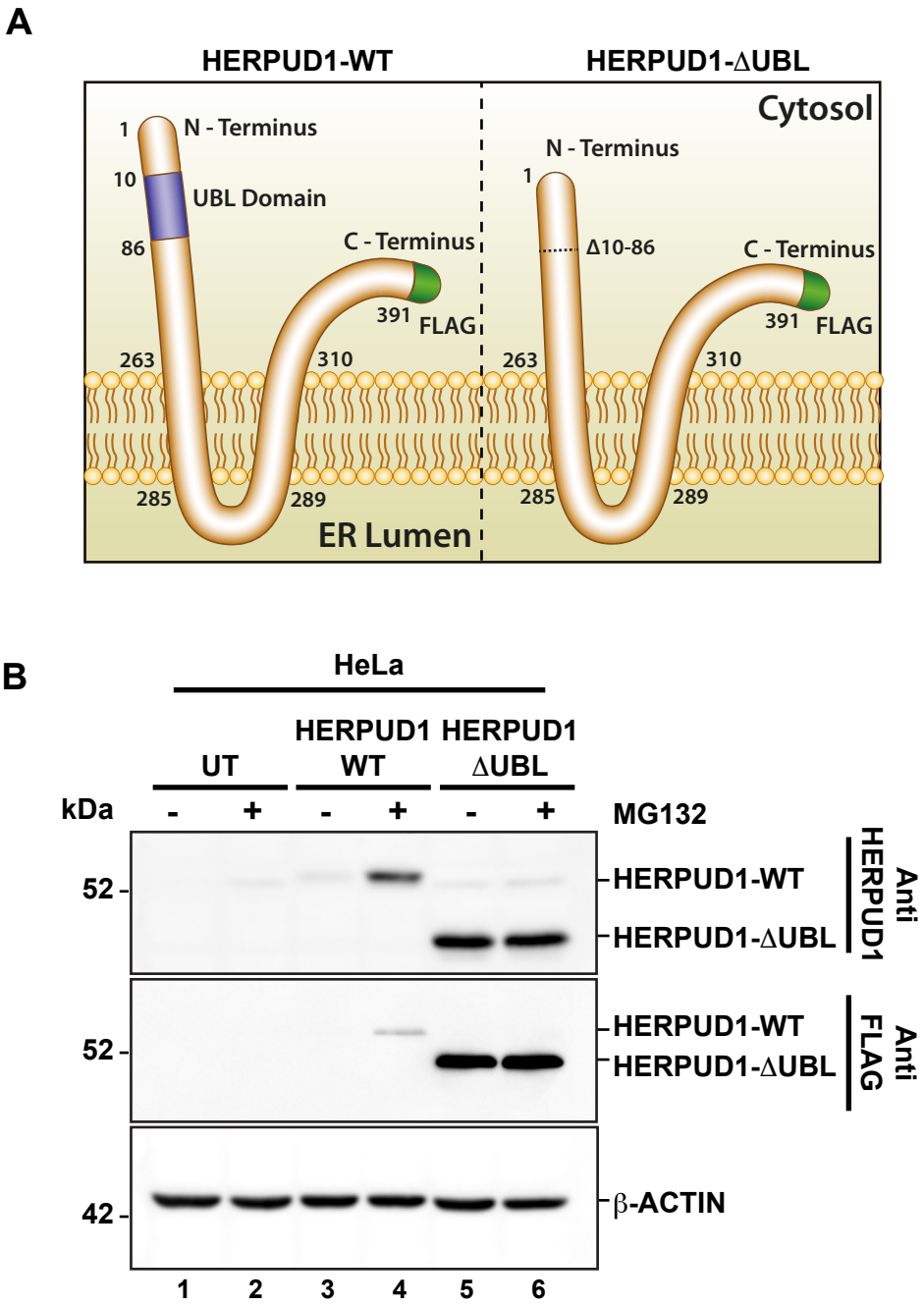
A
HERPUD1-WT
HERPUD1-ΔUBL
Cytosol
1
N - Terminus
10
UBL Domain
86
C - Terminus
391
FLAG
263
310
285
289
ER Lumen
N - Terminus
1
Δ10-86
C - Terminus
391
FLAG
263
310
285
289
B
HeLa
UT
HERPUD1 WT
HERPUD1 ΔUBL
kDa
- + - + - +
MG132
52
HERPUD1-WT
HERPUD1-ΔUBL
Anti HERPUD1
52
HERPUD1-WT
HERPUD1-ΔUBL
Anti FLAG
42
β-ACTIN
1 2 3 4 5 6

Figure 2

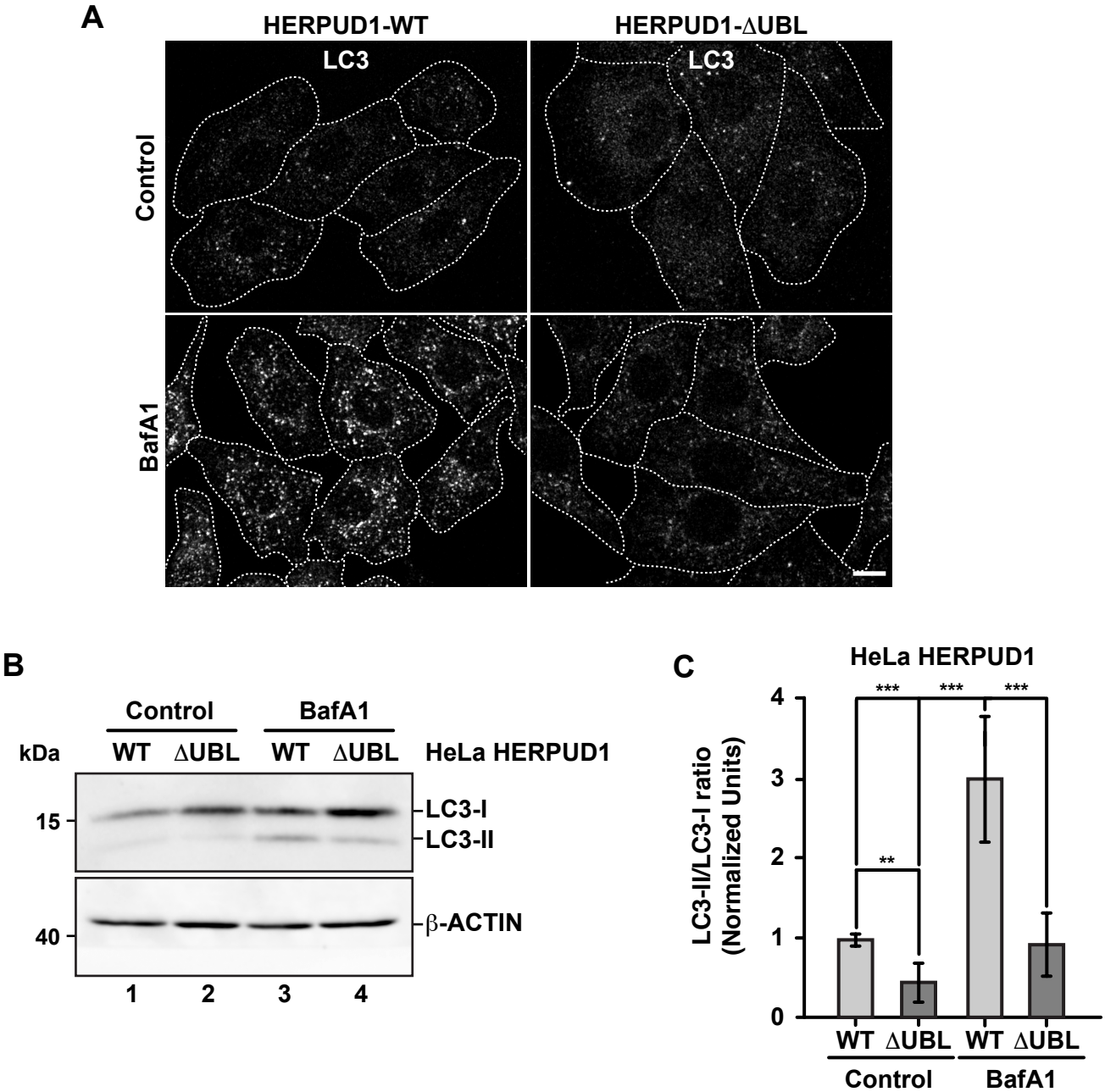
A
HERPUD1-WT
HERPUD1-ΔUBL
LC3
LC3
Control
BafA1
B
Control
BafA1
kDa
WT
ΔUBL
WT
ΔUBL
HeLa HERPUD1
15
LC3-I
LC3-II
40
β-ACTIN
1
2
3
4
C
HeLa HERPUD1
LC3-II/LC3-I ratio
(Normalized Units)
4
3
2
1
0
***
***
***
**
WT
ΔUBL
WT
ΔUBL
Control
BafA1

Figure 3

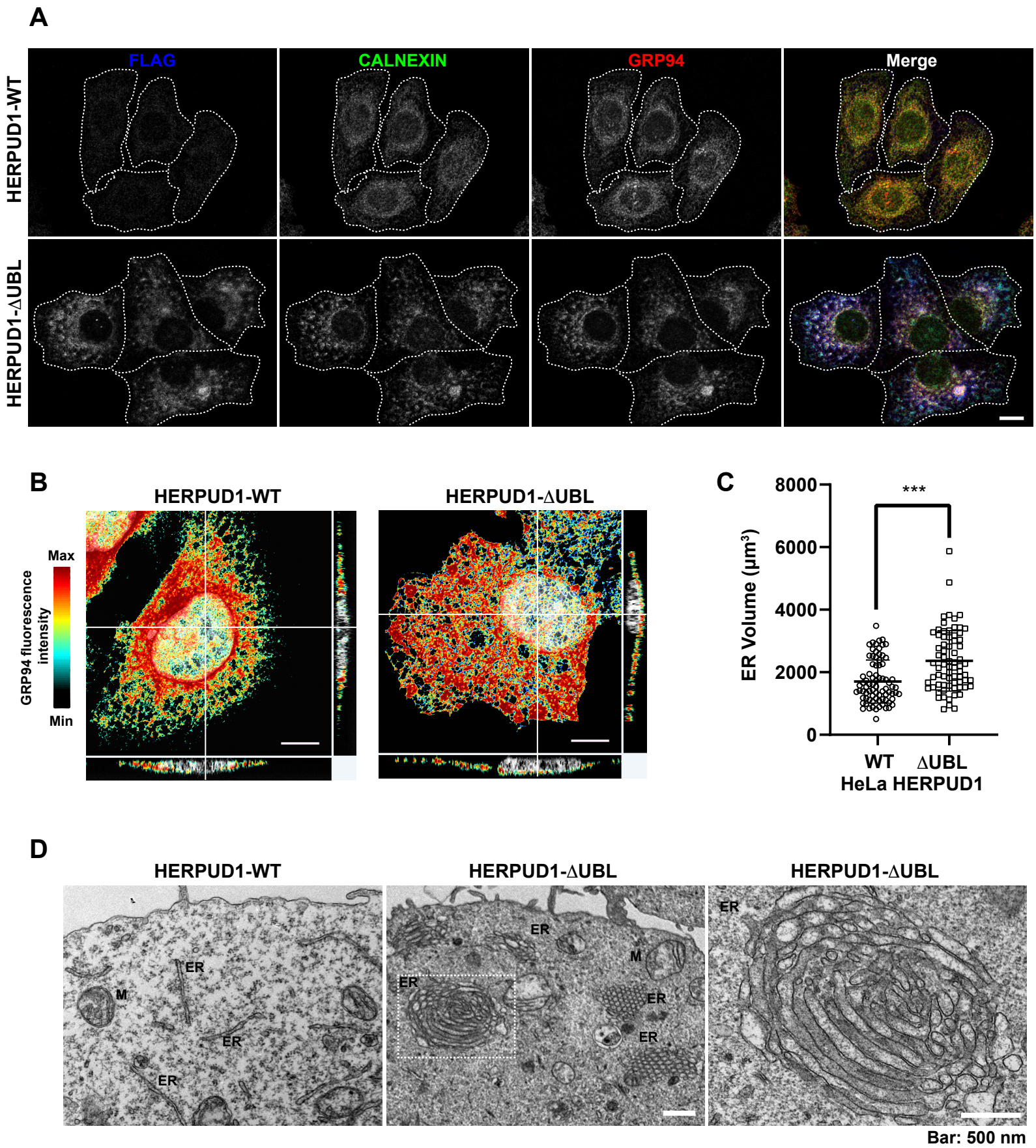
A
FLAG
CALNEXIN
GRP94
Merge
HERPUD1-WT
HERPUD1-ΔUBL
B
HERPUD1-WT
HERPUD1-ΔUBL
Max
Min
GRP94 fluorescence intensity
C
***
ER Volume (μm³)
8000
6000
4000
2000
0
WT
ΔUBL
HeLa HERPUD1
D
HERPUD1-WT
HERPUD1-ΔUBL
HERPUD1-ΔUBL
ER
M
Bar: 500 nm

Figure 4

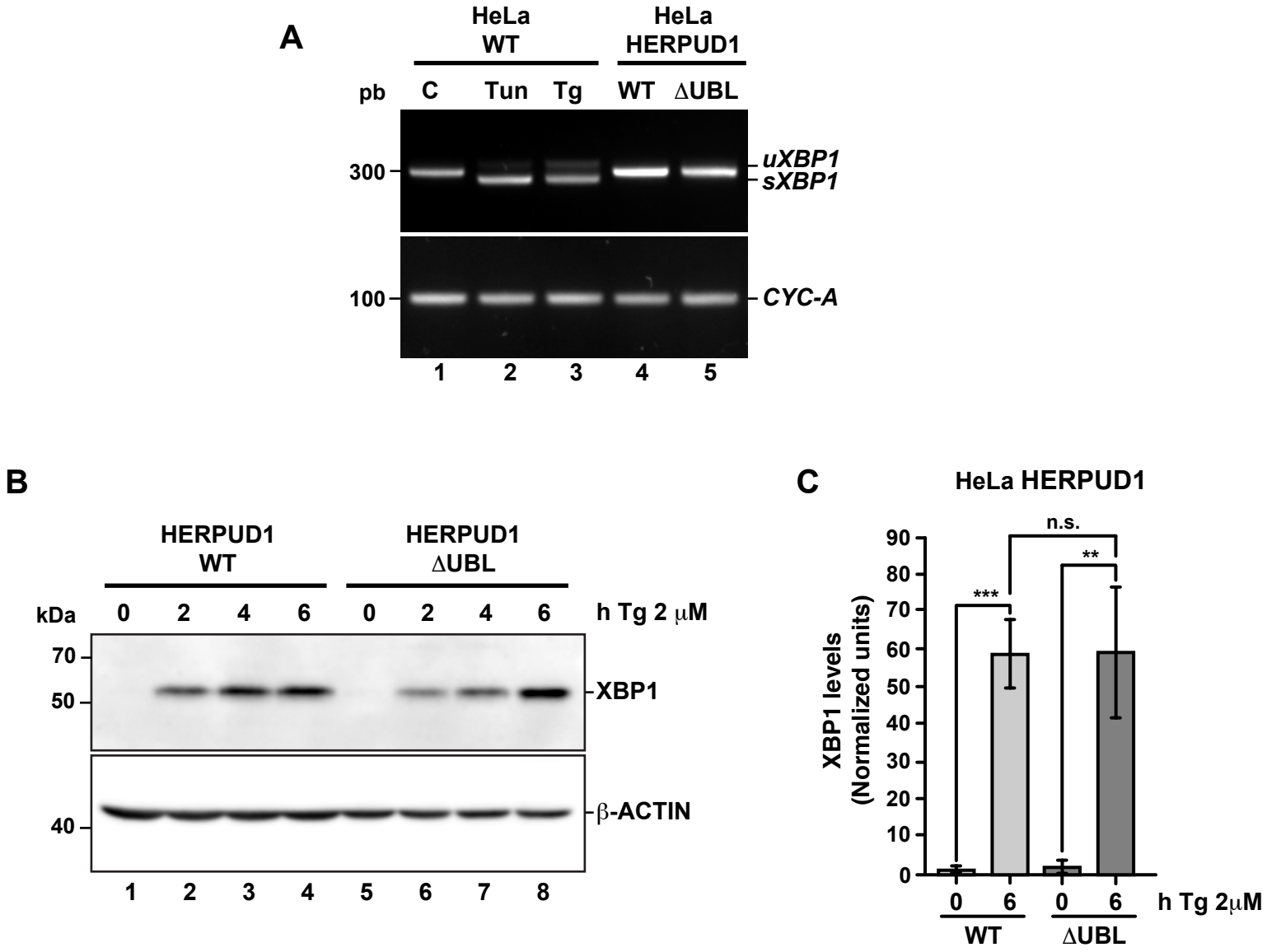
A
HeLa WT
HeLa HERPUD1
pb
C
Tun
Tg
WT
ΔUBL
300
100
uXBP1
sXBP1
CYC-A
1
2
3
4
5
B
HERPUD1 WT
HERPUD1 ΔUBL
kDa
0
2
4
6
0
2
4
6
h Tg 2 μM
70
50
40
XBP1
β-ACTIN
1
2
3
4
5
6
7
8
C
HeLa HERPUD1
n.s.
**
***
XBP1 levels (Normalized units)
90
80
70
60
50
40
30
20
10
0
0
6
0
6
h Tg 2μM
WT
ΔUBL

Figure 5

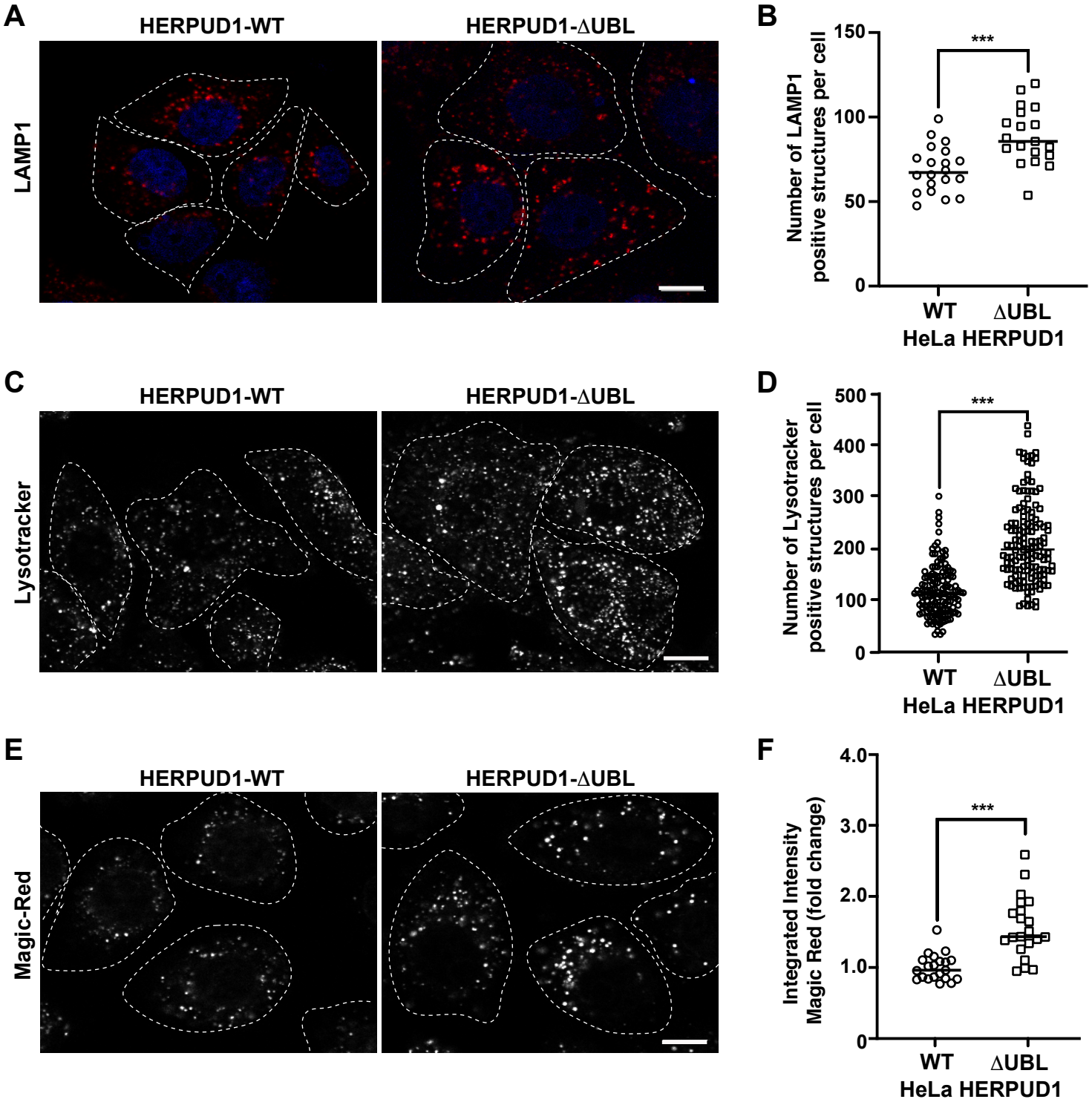
A
HERPUD1-WT
HERPUD1-ΔUBL
LAMP1
B
Number of LAMP1 positive structures per cell
150
100
50
0
***
WT
ΔUBL
HeLa HERPUD1
C
HERPUD1-WT
HERPUD1-ΔUBL
Lysotracker
D
Number of Lysotracker positive structures per cell
500
400
300
200
100
0
***
WT
ΔUBL
HeLa HERPUD1
E
HERPUD1-WT
HERPUD1-ΔUBL
Magic-Red
F
Integrated Intensity Magic Red (fold change)
4.0
3.0
2.0
1.0
0
***
WT
ΔUBL
HeLa HERPUD1

Figure 6

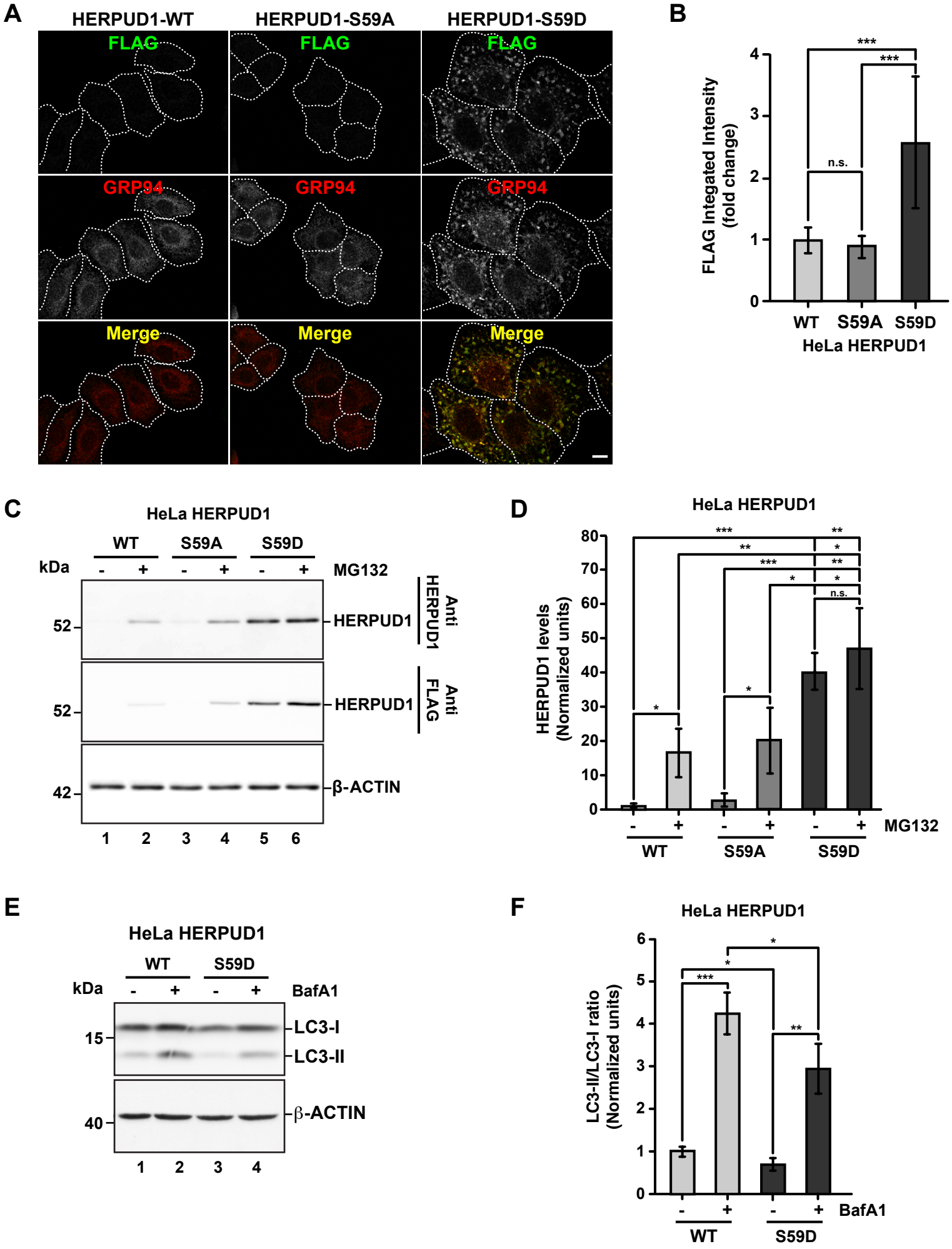
A
HERPUD1-WT
HERPUD1-S59A
HERPUD1-S59D
FLAG
GRP94
Merge
B
FLAG Integated Intensity (fold change)
***
n.s.
WT
S59A
S59D
HeLa HERPUD1
C
HeLa HERPUD1
kDa
MG132
52
42
HERPUD1
β-ACTIN
Anti HERPUD1
Anti FLAG
1 2 3 4 5 6
D
HeLa HERPUD1
HERPUD1 levels (Normalized units)
MG132
E
HeLa HERPUD1
kDa
BafA1
15
40
LC3-I
LC3-II
β-ACTIN
1 2 3 4
F
HeLa HERPUD1
LC3-II/LC3-I ratio (Normalized units)
BafA1

Figure 7

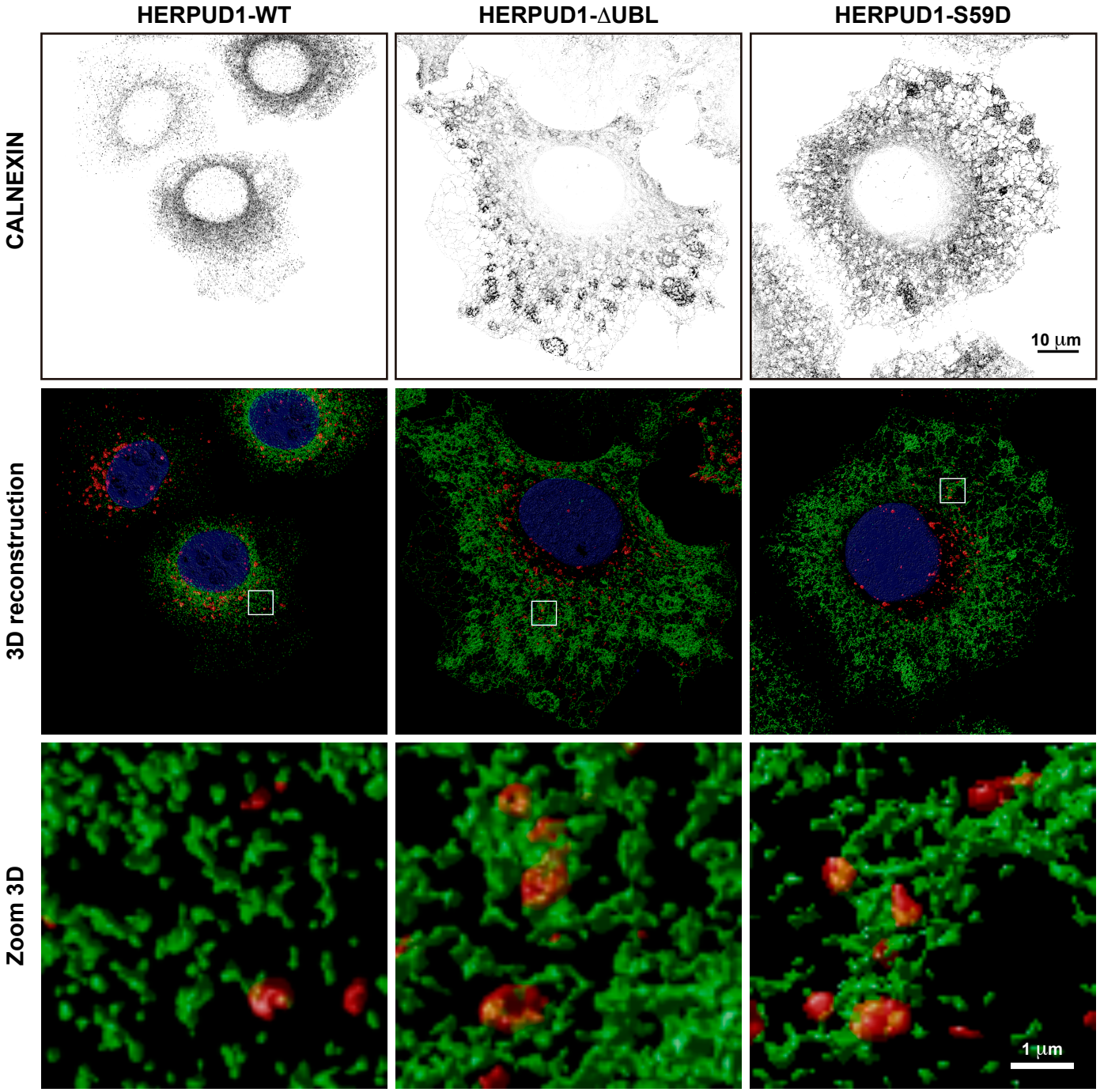
HERPUD1-WT
HERPUD1-ΔUBL
HERPUD1-S59D
CALNEXIN
3D reconstruction
Zoom 3D
10 µm
1 µm

Figure 8

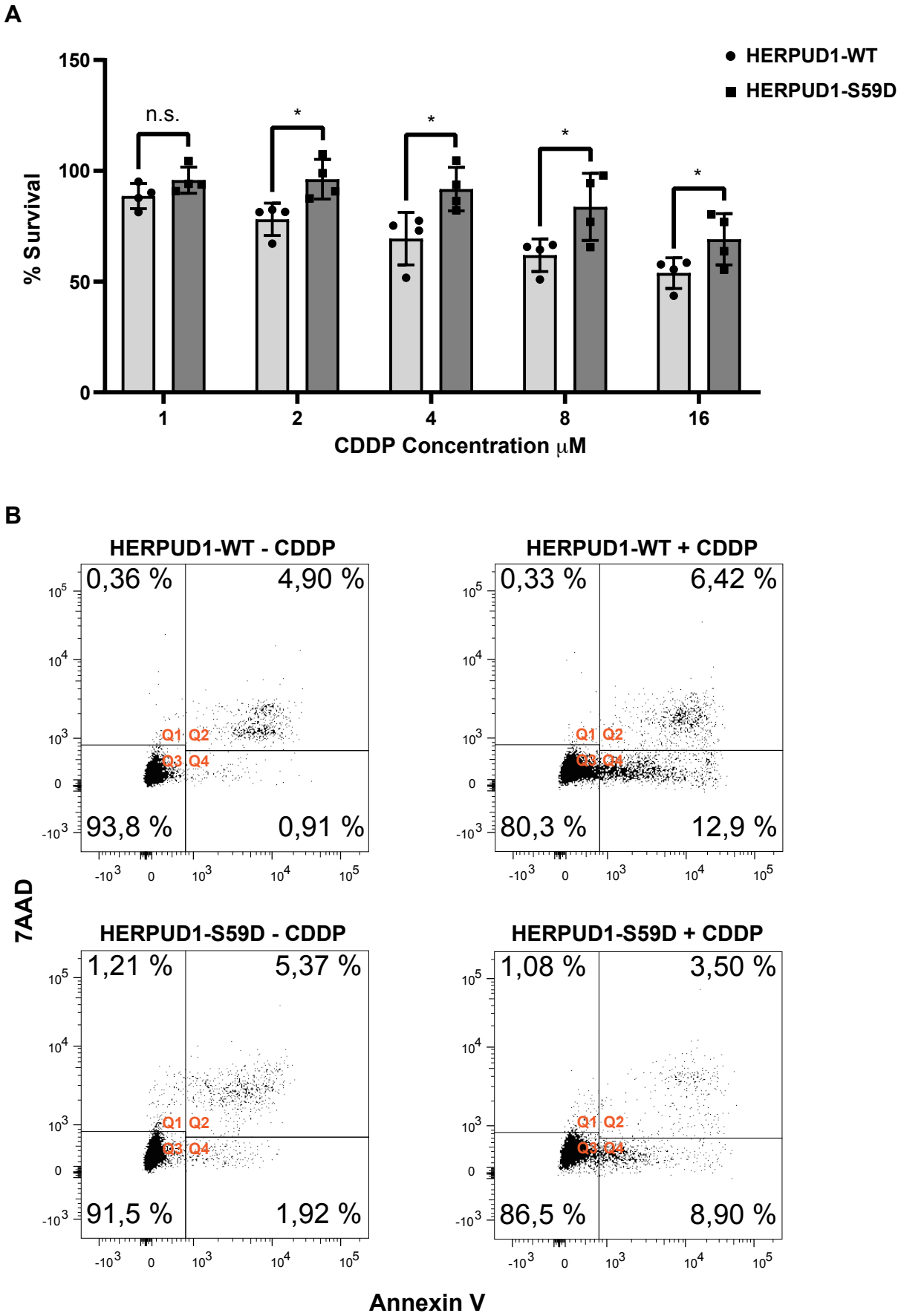
A
HERPUD1-WT
HERPUD1-S59D
% Survival
150
100
50
0
n.s.
*
*
*
*
1
2
4
8
16
CDDP Concentration μM
B
HERPUD1-WT - CDDP
0,36 %
4,90 %
93,8 %
0,91 %
HERPUD1-WT + CDDP
0,33 %
6,42 %
80,3 %
12,9 %
HERPUD1-S59D - CDDP
1,21 %
5,37 %
91,5 %
1,92 %
HERPUD1-S59D + CDDP
1,08 %
3,50 %
86,5 %
8,90 %
Q1
Q2
Q3
Q4
7AAD
Annexin V

Figure 9